NASA Contractor Report 189090
CU-CSSC-91-28

Analysis of Superconducting Electromagnetic Finite Elements Based on a Magnetic Vector Potential Variational Principle

James J. Schuler and Carlos A. Felippa
University of Colorado
Boulder, Colorado

December 1991

NASA

National Aeronautics and
Space Administration

ANALYSIS OF SUPERCONDUCTING ELECTROMAGNETIC FINITE ELEMENTS BASED ON A MAGNETIC VECTOR POTENTIAL VARIATIONAL PRINCIPLE

JAMES J. SCHULER

CARLOS A. FELIPPA

Department of Aerospace Engineering Sciences
and Center for Space Structures and Controls
University of Colorado
Boulder, Colorado 80309-0429, USA

ABSTRACT

We extend electromagnetic finite elements based on a variational principle that uses the electromagnetic four-potential as primary variable. The variational principle is extended to include the ability to predict a non-linear current distribution within a conductor. The extension of this theory is first done on a normal conductor and tested on two different problems. In both problems, the geometry remains the same, but the material properties are different. The geometry is that of a one-dimensional infinite wire. The first problem is merely a linear "control" case used to validate the new theory. The second more interesting problem is made up of linear conductors with varying conductivities. Both problems perform exceedingly well and predict current densities that are accurate to within a few ten-thousandths of a percent of the exact values. The fourth potential is then removed, leaving only the magnetic vector potential, and the variational principle is further extended to predict magnetic potentials, magnetic fields, the number of charge carriers and the current densities within a superconductor. The new element generated by this formulation is then tested on a one-dimensional infinite superconducting wire. The element produces good results for the mean magnetic field, the vector potential and the number of superconducting charge carriers despite a relatively high system condition number. The element did not perform well in predicting the current density. Numerical problems inherent to this formulation are explored and possible remedies to produce better current predicting finite elements are presented.

into complex problems can be made more productive. It centers on the observation that some aspects of the problem are either better understood or less physically relevant than others. These aspects may be then temporarily left alone while efforts are concentrated on the less developed and/or more physically important aspects. The staged treatment is better suited to this approach.

1.2 Mechanical Elements

Mechanical elements for this research have been derived using general variational principles that decouple the element boundary from the interior thus providing efficient ways to work out coupling with non-mechanical fields. The point of departure was previous research into the free-formulation variational principles presented in Ref. [3]. A more general formulation for the mechanical elements, which includes the assumed natural strain formulation, was established and presented in Refs. [4–7]. New representations of thermal fields have not been addressed as standard formulations are considered adequate for the coupled-field phases of this research.

2. ELECTROMAGNETIC ELEMENTS

The development of electromagnetic (EM) finite elements has not received to date the same degree of attention given to mechanical and thermal elements. Part of the reason is the widespread use of analytical and semianalytical methods in electrical engineering. These methods have been highly refined for specialized but important problems such as circuits and waveguides. Thus the advantages of finite elements in terms of generality have not been enough to counterweight established techniques. Much of the EM finite element work to date has been done in England and is well described in the surveys by Davies [8] and Trowbridge [9]. The general impression conveyed by these surveys is one of an unsettled subject, reminiscent of the early period (1960-1970) of finite elements in structural mechanics. A great number of formulations that combine flux, intensity, and scalar potentials are described with the recommended choice varying according to the application, medium involved (polarizable, dielectric, semiconductors, etc.) number of space dimensions, time-dependent characteristics (static, quasi-static, harmonic or transient) as well as other factors of lesser importance. The possibility of a general variational formulation has apparently not been recognized.

In the present work, the derivation of electromagnetic (EM) elements is based on a variational formulation that uses the four-potential as primary variable. The electric field is represented by a scalar potential and the magnetic field by a vector potential. The formulation of this variational principle proceeds along lines previously developed for the acoustic fluid problem [10,11].

The main advantages of using potentials as primary variables as opposed to the more conventional EM finite elements based on intensity and/or flux fields are, in order or importance:

1. Interface discontinuities are automatically taken care of without any special interven-

tion.

2. No approximations are invoked *a priori* since the general Maxwell equations are used.

3. The number of degrees of freedom per finite element node is kept modest as the problem dimensionality increases.

4. Coupling with the mechanical and thermal fields, which involves derived fields, can be naturally evaluated at the Gauss points at which derivatives of the potentials are evaluated.

The problems which are presented in this paper only have one geometry, that of an infinitely long cylindrical wire (see Fig. 1). The problems that are examined are:

1. Infinite conductor with the same conductivity between elements.

2. Infinite conductor with different conductivities between elements.

3. Infinite superconductor.

3. LINEAR FINITE ELEMENT WITH CURRENT PREDICTION

In the previous development of electromagnetic finite elements, the current distribution, **J**, has always been assumed to be given. Unfortunately, **J** for a superconductor is not linear, and with the exception of a few special cases, unknown. Since it is not known *a priori* what the current distribution for a superconducting element will be, these elements must have the ability to predict the current density **J**, as well as the magnetic potential **A**. The starting point in developing a superconducting element is to build a linear element with current prediction capabilites. Because current density varies from element to element in a superconductor, our new linear element should be able to model a current density that changes from element to element. This occurs for a linear media when the material conductivity, σ, changes from element to element.

3.1 Finite Element for a Linear Conductor

The potential energy functional for a linear conductor is given by

$$U = \int_V dV \left\{ \frac{1}{2\mu} (\nabla \times \mathbf{A})^2 - \frac{1}{2}\epsilon(-\nabla\phi)^2 - \mathbf{J}^T \mathbf{A} \right\} \tag{1}$$

The constitutive relation (Ohm's law) is:

$$\mathbf{J} = -\sigma\nabla\phi \tag{2}$$

where σ is the material conductivity.

Substitution of the (2) into (1) yields

$$U = \int_V dV \left\{ \frac{1}{2\mu} (\nabla \times \mathbf{A})^2 - \frac{1}{2}\epsilon \left(\frac{\mathbf{J}}{\sigma}\right)^2 - \mathbf{J}^T \mathbf{A} \right\} \tag{3}$$

Variation of the above gives

$$\delta U = \int_V dV \left\{ \frac{1}{\mu} (\nabla \times \delta\mathbf{A})^T (\nabla \times \mathbf{A}) - \epsilon \left(\frac{\delta\mathbf{J}}{\sigma}\right)^T \left(\frac{\mathbf{J}}{\sigma}\right) - \delta\mathbf{J}^T \mathbf{A} - \mathbf{J}^T \delta\mathbf{A} \right\} \tag{4}$$

For a one-dimensional axisymmetric problem where the only non-zero components of $\mathbf{A}$ and $\mathbf{J}$ are A_z and J_z, this reduces to

$$\delta U = \int_V dV \left\{ \frac{1}{\mu} \left(\frac{\partial \delta A_z}{\partial r}\right)\left(\frac{\partial A_z}{\partial r}\right) - \frac{\epsilon}{\sigma^2}(\delta J_z)^T (J_z) - \delta J_z A_z - J_z \delta A_z \right\} \tag{5}$$

Integration by parts produces:

$$\delta U = \int_V dV \left\{ \delta A_z \left(-\frac{1}{\mu}\frac{\partial}{\partial r}\left(r\frac{\partial A_z}{\partial r}\right) - J_z\right) - \delta J_z \left(\frac{\epsilon}{\sigma^2} J_z + A_z\right) + \frac{1}{\mu}\frac{\partial A_z}{\partial r} r \delta A_z(r)\Big|_{r_i}^{r_j} \right\} \tag{6}$$

This is appropriate if $\mathbf{J}$ and σ are continuous. If σ is discontinuous, i.e., varies from element to element, then we need to examine what happens at element boundaries. Since the energy functional has variational index $m = 0$ for $\mathbf{J}$, we may approximate an element current density, $\mathbf{J}_i^e$, as a step function. Maxwell's equations require that $\nabla \times \mathbf{E} = \sigma^{-1}\nabla \times \mathbf{J} = 0$. The one-dimensional discretized equation is

$$\sigma_i^{-1} J_{z_i}^e \frac{\partial}{\partial r} u(r_i - r_{i-1})\big|_{r_i} = \sigma_{i+1}^{-1} J_{z_{i+1}}^e \frac{\partial}{\partial r} u(r_{i+1} - r_i)\big|_{r_i} \tag{7}$$

$$\sigma_i^{-1} J_{z_i}^e \delta(r_i - r_{i-1})\big|_{r_i} = \sigma_{i+1}^{-1} J_{z_{i+1}}^e \delta(r_{i+1} - r_i)\big|_{r_i} \tag{8}$$

$$\sigma_i^{-1} J_{z_i}^e = \sigma_{i+1}^{-1} J_{z_{i+1}}^e \tag{9}$$

where $u(r_j - r_i)$ and $\delta(r_j - r_i)$ are the Heavyside step and Dirac delta functions respectively. This boundary condition equation, weighted by a Lagrangian multiplier, is added to the original functional. These multipliers will be denoted by $\lambda_{l_i}^e$, where i is the number of the boundary between two adjacent conducting elements.

The last requirement on this system of equations comes from the law of charge conservation. With I being the total current flowing through a surface Γ, and $\hat{n}$ the unit normal, this law is

$$I = \int_\Gamma \mathbf{J} \cdot \hat{\mathbf{n}} d\Gamma \tag{10}$$

or in discretized form

$$I - \sum_{k=1}^{numel} \int_{\Gamma_k} \mathbf{J}_k \cdot \hat{\mathbf{n}}_k d\Gamma_k = 0 \tag{11}$$

Multiplying this equation by the global Lagrangian multiplier λ_g and adding to the modified energy funcional gives, in discretized form

$$U = \sum_{m=1}^{numel} \int_{V_m^e} dV_m^e \left\{ \frac{1}{2\mu} (\nabla \times \mathbf{N}_m \mathbf{A}_m^e)^T (\nabla \times \mathbf{N}_m \mathbf{A}_m^e) - \frac{\epsilon}{2} \left(\frac{\mathbf{J}_m^e}{\sigma_m}\right)^T \left(\frac{\mathbf{J}_m^e}{\sigma_m}\right) - \mathbf{J}_m^{eT} \mathbf{N}_m \mathbf{A}_m^e \right\}$$
$$+ \sum_{i=1}^{numel-1} \lambda_{l_i}^e (\sigma_i^{-1} J_{z_i}^e - \sigma_{i+1}^{-1} J_{z_{i+1}}^e) + \lambda_g \left(I - \sum_{k=1}^{numel} \int_{\Gamma_k} \mathbf{J}_k \cdot \hat{\mathbf{n}}_k d\Gamma_k \right) \tag{12}$$

Next we change I to $I_o + \lambda I_L$, where I_o is the initial current value, I_L is the amount of loading current added to the system, and λ is the control parameter. The variations of the modified energy functional are then taken with respect to $\mathbf{A}^e$, $\mathbf{J}^e$, $\lambda_{l_i}^e$, λ_g, and λ to get the internal and external force vectors.

The internal force vector $\mathbf{f}$ is

$$\frac{\partial U}{\partial \mathbf{v}} + \mathbf{p} = \mathbf{f} = \sum_{m=1}^{numel} \int_{V_m^e} dV_m^e \left(\frac{1}{\mu} \frac{\partial \mathbf{N}_m}{\partial r}^T \frac{\partial \mathbf{N}_m}{\partial r} \mathbf{A}_m^e - \mathbf{N}_m^T J_{z_m}^e \right)$$
$$- \sum_{m=1}^{numel} \int_{V_m^e} dV_m^e (\mathbf{N}_m \mathbf{A}_m^e + \epsilon \sigma^{-2} J_{z_m}^e)$$
$$+ \sum_{i=1}^{numel-1} \lambda_{l_i}^e (\sigma_i^{-1} - \sigma_{i+1}^{-1}) + \sum_{i=1}^{numel-1} (\sigma_i^{-1} J_{z_i}^e - \sigma_{i+1}^{-1} J_{z_{i+1}}^e)$$
$$- \lambda_g \left(\sum_{k=1}^{numel} \int_{\Gamma_k} d\Gamma_k \right) + \left(I_o - \sum_{k=1}^{numel} \int_{\Gamma_k} J_{z_k} d\Gamma_k \right) \tag{13}$$

where vector $\mathbf{v}$ includes the degrees of freedom. The external force vector $\mathbf{p}$ is

$$\mathbf{p} = \lambda \mathbf{q} = -\lambda \frac{\partial^2 U}{\partial \mathbf{v} \partial \lambda} = -\lambda I_L \mathbf{e}_{\lambda_g} \tag{14}$$

where $\mathbf{q}$ is the loading vector and $\mathbf{e}_{\lambda_g}$ is the vector with all zero components except the one associated with the degree of freedom at λ_g, which is one.

6

Letting **w** be the vector of incremental velocities then

$$\mathbf{w} = \left\{ \begin{array}{c} \Delta A_{z_1} \\ \Delta A_{z_2} \\ \vdots \\ \Delta A_{z_{numel}} \\ \Delta J_{z_1} \\ \Delta \lambda l_1 \\ \Delta J_{z_2} \\ \Delta \lambda l_2 \\ \vdots \\ \Delta J_{z_{numel-1}} \\ \Delta \lambda l_{numel-1} \\ \Delta \lambda_g \end{array} \right\}$$

Since the tangent stiffness matrix, **K**, is not separable on an element level, **K**Δ**v** is presented here rather than the expression for **K**. The product is

$$\mathbf{K}\Delta\mathbf{v} = \sum_{m=1}^{numel} \int_{V_m^e} dV_m^e \left(\frac{1}{\mu} \frac{\partial \mathbf{N}_m}{\partial r}^T \frac{\partial \mathbf{N}_m}{\partial r} \Delta \mathbf{A}_m^e - \mathbf{N}_m^T \Delta J_{z_m}^e \right)$$

$$- \sum_{m=1}^{numel} \int_{V_m^e} dV_m^e \left(\mathbf{N}_m \Delta \mathbf{A}_m^e + \epsilon \sigma^{-2} \Delta J_{z_m}^e \right)$$

$$+ \sum_{i=1}^{numel-1} \Delta \lambda_{l_i}^e (\sigma_i^{-1} - \sigma_{i+1}^{-1}) + \sum_{i=1}^{numel-1} (\sigma_i^{-1} \Delta J_{z_i}^e - \sigma_{i+1}^{-1} \Delta J_{z_{i+1}}^e)$$

$$- \Delta \lambda_g \left(\sum_{k=1}^{numel} \int_{\Gamma_k} d\Gamma_k \right) - \sum_{k=1}^{numel} \int_{\Gamma_k} \Delta J_{z_k} d\Gamma_k \tag{15}$$

3.2 Nonconducting Element

For an element outside of the conductor (for example, free space) $\mathbf{J}^e$ equals zero, and consequently the energy functional reduces to

$$U = \sum_{m=1}^{numel} \int_{V_m^e} dV_m^e \left\{ \frac{1}{2\mu} (\nabla \times \mathbf{N}_m \mathbf{A}_m^e)^T (\nabla \times \mathbf{N}_m \mathbf{A}_m^e) \right\} \tag{16}$$

So on an *elemental* level, in the one-dimensional case, $\mathbf{f}^e$, $\mathbf{q}^e$, and $\mathbf{K}^e$ become

$$\mathbf{f}^e = \int_{V_m^e} dV_m^e \left\{ \frac{1}{\mu} \left(\frac{\partial \mathbf{N}_m}{\partial r} \right)^T \left(\frac{\partial \mathbf{N}_m}{\partial r} \mathbf{A}_m^e \right) \right\} \qquad (17)$$

$$\mathbf{q}^e = \mathbf{0} \qquad (18)$$

$$\mathbf{K}^e = \int_{V_m^e} dV_m^e \left\{ \frac{1}{\mu} \left(\frac{\partial \mathbf{N}_m}{\partial r} \right)^T \left(\frac{\partial \mathbf{N}_m}{\partial r} \right) \right\} \qquad (19)$$

4. NUMERICAL VALIDATION OF LINEAR ELEMENT

4.1 The Finite Element Model

The finite element formulation derived in the previous section has been applied to two test problems described below. Both problems are treated with one-dimensional axisymmetric elements. Each bar element has two end points, one interior node and a common shared global node. These nodes are defined by their axial position r_j^e. The two end nodes have one degree of freedom each corresponding to A_{zi} and A_{zj}. From these values the magnetic potential components are interpolated with the standard linear shape functions, which provide the C^o continuity required by the variational formulation. The interior node is placed at the center of the element and the global node at the end of the finite element mesh. Neither of these nodes carry any physical signifigance and are used solely to provide the extra degrees of freedom assigned to the two Lagrangian multipliers and the degree of freedom assigned to $\mathbf{J}^e$. $\mathbf{J}^e$ and λ_f^e are carried on the center node and λ_g is carried on the common node. Consequently, each element has $2 \times 1 + 2 + 1 = 5$ degrees of freedom.

For the calculation of the element stiffnesses and force vectors, it is assumed that the permeability μ and current densities are uniform over the element. The desired stiffness matrix and force vector are calculated by numerical quadrature using a 2 point Gauss formula.

4.2 Applying Boundary Conditions

The finite element mesh is necessarily terminated at a finite size. For the two test problems, the outer radial end of the mesh is defined as the truncation radius $r = R_T$. The outer radial end of the conductor's mesh is defined as the wire radius $r = R_{wire}$. Since current is only carried in the conductor, the degrees of freedom for $\mathbf{J}^e$ between R_{wire} and R_T are constrained to zero. Constraining $\mathbf{A}$ to zero at R_T causes both boundary terms in equation (6) to disappear. Notice that constraining $\mathbf{A}$ to be zero at $r = 0$ does not remove the outer

8

boundary term in equation (6). This is shown in section 5.1, where $A(r=0)$ is required to be zero.

4.3 Assembly, Solution and Field Recovery

The components of the element stiffness matrix corresponding to the summations from 1 to $numel$ in equation 15 are first calculated and inserted into the master stiffness matrix. The components for the remaining two summations are next determined and added to the master tangent stiffness matrix. This is done in an element by element fashion until the complete master tangent stiffness matrix is assembled. The loading force vector is assembled in an element by element fashion following standard finite element technique. The boundary conditions are set as explained in the previous section. The modified master equations modified for B.C. are processed by a standard symmetric skyline solver, which provides the value of the magnetic potential at the mesh nodes, and the mean current density over each element.

The physical quantity of main interest is not the potential, but the magnetic field B_θ. This is obtained by discretizing A as follows. Since A is only a function of r, $B_\theta = -(\partial N/\partial r)A_z^e$. This represents the mean value of B over the volume of the element. In previous papers [15, 16], extrapolation of this value to the endpoints was tried with little success and was not tried here. Consequently, the value obtained for B is plotted as a step function over the elements in our figures.

The ability of the potential formulation to accurately model the discontinuity in the B field at a conductor/free space interface has already been established in previous works [15, 16]. For this reason, in both test problems μ is set equal to 1 inside the conductor and in the free space surrounding it. The first test problem sets all the σ_i's to one, and the second problem sets the σ_i for the element equal to the element number.

4.4 Problem 1: Equal Conductivities

The first test problem is identical to that reported in Schuler and Felippa [15] with a one-dimensional axisymmetric discretization. As shown in Figure 1, it consists of a wire conductor of radius R_{wire} transporting a total current $I = 1$ in the z direction. For all of the problems reported here, the elements were assumed to have a unit thickness in the z direction. Since none of the desired quantities vary in the z direction this is a valid assumption. The radial direction is discretized with N_{wire} elements inside the wire and N_{free} elements outside the wire in free space. The mesh is truncated at a "truncation radius" R_T, where the potential A_z is set equal to zero. Other boundary conditions are set as previously defined.

The results obtained with $R_T = 2R_{wire}$, $N_{wire} = 20$, $N_{free} = 20$ for the potentials matched those generated by our previous linear electro-magnetic finite elements [15, 16]. Because

a potential may vary by a constant, it is not necessary for the two curves to lie one upon another, only that they have the same shape. Figure 3 shows the curves obtained for the exact and computed solutions for the potential and verifies that these curves are almost an exact match. Figure 2 shows the analytical and computed solutions for the current densities. The result obtained for the computed current density is lower than the true value by less than one ten thousandth of a percent, thus providing a check on the element calculations. Because these results are so close to the exact solution, they are plotted as a series of points, rather than a line, so that they may be distinguised from the exact solution.

4.5 Problem 2: Different Conductivities

This problem's geometry, R_T, R_{wire}, N_{free} and N_{wire} are the same as that reported above. The only difference is that now the element conductivity is set to the element number. The values obtained for the current densities were just as good as those obtained in the first test example. Similarly, the values obtained for the potentials and magnetic fields gave results with an order of accuracy of previous finite elements. The computed potential varied from the analytical potential by an almost constant value, as Figure 6 shows, and the curve for the true value of the magnetic field intersected the middle of the top of the "step" of the computed solution. The magnetic field was represented as a step function here, unlike our results in previous papers. This was done to more accurately portray that the computed B field is the mean value for the true B field over the element. The computed value does not go to zero at the element boundary ($r = 0$), as expected, since it is the mean over the first element. Close inspection of Figures 4 and 7 reveals that the true value does not intersect the middle of the "step" there, showing that as we get closer to the center of the conductor, the computed value is higher than it should be. Numerical experiments reveal that if a finer and finer mesh is used, that the computed value converges closer to the true value, as expected, therefore verifying the validity of this model to accurately calculate A, B, and J.

4.6 Conclusions with Respect to a Current Predicting Element

The results obtained in the previous two problems show that it is possible to extend previously derived finite element formulations for static and quasi-static magnetic fields to cases where the current distribution in the element is unknown. This is particularly encouraging since this means that it should be possible to solve problems where material and geometric nonlinearities preclude a linear current distribution. It also means that whereas before a knowledge of how the current was distributed in a conductor was needed, with the new formulation, all that is needed is the total current I through the conductor, its material properties μ and σ, and the conductor geometry.

Table 1   Theory Nomenclature

Symbol	Quantities
$\alpha,\ \beta$	Temperature dependent material parameters
ψ	Analagous to a wave/position function in particle mechanics
$|\psi|^2$	Number of superconducting charge carriers per unit volume
ψ^*	Complex conjugate of ψ
q^*	Effective charge on charge carriers
m^*	Effective mass on charge carriers
$\hbar$	Planck's constant divided by $2\ \pi$
A	Magnetic potential vector
B	Total magnetic field
J	Current distribution
λ_L	Lagrangian multiplier whose domain is over the volume of interest
F_s	Helmholtz free energy of superconducting state
F_n	Helmholtz free energy of normal state
ΔF	$F_s - F_n$

Having successfully extended our formulation to include the ability to predict current densities, we next attempt to solve the problem of a nonlinear conductor, the superconductor.

5. SUPERCONDUCTING F.E. WITH CURRENT PREDICTION

This section presents the basic theory for superconductivity and how the constraints and finite elements for one-dimensional superconducting problems were developed. Table 1 presents the nomenclature for the quantities used in this work.

5.1 The Helmholtz Free Energy for a Superconductor

In the general vicinity of the transition or critical temperature for a type I or II superconductor, the change in the Helmholtz free energy (F) can be approximated as

$$\Delta F = F_s - F_n = \int_V dV \left\{ -\alpha|\psi|^2 + \tfrac{1}{2}\beta|\psi|^4 + \frac{1}{2m^*}|(-i\hbar\nabla - q^*\mathbf{A})\psi|^2 + \tfrac{1}{2}\mathbf{B}\cdot\mathbf{H} \right\} \quad (20)$$

in S.I. units [17], where the quantities α, β and ψ are defined in Table 1. The first two terms represent a typical Landau expansion of the Helmholtz free energy for a second order phase transition. The third term represents the total momentum of the charge carrier. The $-i\hbar\nabla$ term is analogous to the dynamic (kinetic) momentum of a quantum wave-like particle[†]; the q^*A term represents the field momentum [13, p. 633; 14, pp. 105-108].

Using the identities, $\mathbf{B} = \mu_o\mathbf{H}$, and $\mathbf{B} = \nabla \times \mathbf{A}$, the last term, which represents the field energy, can be replaced by

$$\frac{1}{2\mu_o}(\nabla \times \mathbf{A})^2 \tag{21}$$

The material's magnetic permeability μ, is set to μ_o, the value of the permeability in free space. This value is chosen because the field energy term represents the magnetic energy in free space, and the other three terms are corrections to that energy resulting from material and dynamic effects. Unlike a linear material, corrections to the field energy in a superconductor cannot be accounted for by an appropriate choice of a constant μ. The magnetic permeability within the conductor is now a function of the spatial coordinates and is no longer a constant.

Expanding ΔF in terms of ψ and ψ^* gives

$$\Delta F = \int_V dV \left\{ -\alpha\psi\psi^* + \tfrac{1}{2}\beta(\psi\psi^*)^2 + \frac{1}{2m^*}(-i\hbar\nabla^T\psi - q^*\mathbf{A}^T\psi) \right.$$
$$\left. (i\hbar\nabla\psi^* - q^*\mathbf{A}\psi^*) + \frac{1}{2\mu_o}(\nabla \times \mathbf{A})^T(\nabla \times \mathbf{A}) \right\} \tag{22}$$

Taking $\psi = \psi_R + \psi_I$, $\psi^* = \psi_R - \psi_I$, where ψ_R represents the real part of the order parameter and ψ_I the imaginary part, gives

$$\Delta F = \int_V dV \left\{ -\alpha(\psi_R{}^2 + \psi_I{}^2) + \tfrac{1}{2}\beta(\psi_R{}^2 + \psi_I{}^2)^2 \right.$$
$$+ \frac{1}{2m^*}(-i\hbar\nabla^T(\psi_R + i\psi_I) - q^*\mathbf{A}^T(\psi_R + i\psi_I))(i\hbar\nabla(\psi_R - i\psi_I) - q^*\mathbf{A}(\psi_R - i\psi_I))$$
$$\left. + \frac{1}{2\mu_o}(\nabla \times \mathbf{A})^T(\nabla \times \mathbf{A}) \right\}$$
$$= \int_V dV \left\{ -\alpha(\psi_R{}^2 + \psi_I{}^2) + \tfrac{1}{2}\beta(\psi_R{}^2 + \psi_I{}^2)^2 + \tfrac{1}{2}(\frac{\hbar^2}{m^*}(\nabla^T\psi_R\nabla\psi_R + \nabla^T\psi_I\nabla\psi_I) \right.$$
$$+ 2\frac{q^*\hbar}{m^*}\mathbf{A}^T(\nabla\psi_R\psi_I - \nabla\psi_I\psi_R) + \frac{q^{*2}}{m^*}\mathbf{A}^T\mathbf{A}(\psi_R{}^2 + \psi_I{}^2))$$
$$\left. + \frac{1}{2\mu_o}(\nabla \times \mathbf{A})^T(\nabla \times \mathbf{A}) \right\} \tag{23}$$

[†] A good example is a one-dimensional particle in an infinitely deep energy well. The $-i\hbar\nabla$ term in our functional is similar, in theory, to the momentum of the particle in the well.

The first variation of ΔF with respect to ψ_R is

$$\delta\Delta F(\delta\psi_R) = \int_V dV\left\{\delta\psi_R\left(-2\alpha\psi_R + 2\beta(\psi_R{}^2 + \psi_I{}^2)\psi_R - \frac{q^*\hbar}{m^*}\nabla\psi_I\mathbf{A}^T + \frac{q^{*2}}{m^*}\mathbf{A}^T\mathbf{A}\psi_R\right) + \right.$$
$$\left.\nabla\delta\psi_R\left(\frac{\hbar^2}{m^*}\nabla^T\psi_R + \frac{q^*\hbar}{m^*}\mathbf{A}^T\psi_I\right)\right\}$$
$$= \int_V dV\left\{\delta\psi_R\left(-2\alpha\psi_R + 2\beta(\psi_R{}^2 + \psi_I{}^2)\psi_R - \frac{q^*\hbar}{m^*}\nabla\psi_I\mathbf{A}^T + \frac{q^{*2}}{m^*}\mathbf{A}^T\mathbf{A}\psi_R + \right.\right.$$
$$\left.\left.\nabla\left(\frac{\hbar^2}{m^*}\nabla^T\psi_R + \frac{q^*\hbar}{m^*}\mathbf{A}^T\psi_I\right)\right)\right\} +$$
$$\int_\Gamma d\Gamma\hat{n}^T\left\{\left(\frac{\hbar^2}{m^*}\nabla\psi_R + \frac{q^*\hbar}{m^*}\mathbf{A}\psi_I\right)\delta\psi_R\right\}$$

$$(24)$$

The variation with respect to ψ_I is

$$\delta\Delta F(\delta\psi_I) = \int_V dV\left\{\delta\psi_I\left(-2\alpha\psi_I + 2\beta(\psi_R{}^2 + \psi_I{}^2)\psi_I + \frac{q^*\hbar}{m^*}\nabla\psi_R\mathbf{A}^T + \frac{q^{*2}}{m^*}\mathbf{A}^T\mathbf{A}\psi_I + \right.\right.$$
$$\left.\left.\nabla\left(\frac{\hbar^2}{m^*}\nabla^T\psi_I - \frac{q^*\hbar}{m^*}\mathbf{A}^T\psi_R\right)\right)\right\} +$$
$$\int_\Gamma d\Gamma\hat{n}^T\left\{\left(\frac{\hbar^2}{m^*}\nabla\psi_I - \frac{q^*\hbar}{m^*}\mathbf{A}\psi_R\right)\delta\psi_I\right\}$$

$$(25)$$

The boundary terms in the last two equations represent the net momentum exchange between the B field and $|\psi|$ at the boundaries. At the inner boundary, we expect the value of ψ to approach a constant for a bulk superconductor. Therefore we require that A go to zero. At the outer boundary, we require that there be no superconducting flux into free space; to ensure this we set ψ equal to zero there.

The variation with respect to A (again in one dimension) is

13

$$\delta\Delta F(\delta \mathbf{A}) = \int_V dV \left\{ \delta \mathbf{A} \left(\frac{q^* \hbar}{m^*} (\nabla^T \psi_R \psi_I - \nabla^T \psi_I \psi_R) + \frac{q^{*2}}{m^*} \mathbf{A}^T (\psi_R{}^2 + \psi_I{}^2) \right) + \right.$$

$$\left. \frac{1}{\mu_o} (\nabla \times \delta \mathbf{A})^T (\nabla \times \mathbf{A}) \right\}$$

$$= \int_V dV \left\{ \delta \mathbf{A} \left(\frac{q^* \hbar}{m^*} (\nabla^T \psi_R \psi_I - \nabla^T \psi_I \psi_R) + \frac{q^{*2}}{m^*} \mathbf{A}^T (\psi_R{}^2 + \psi_I{}^2) + \right. \right. \quad (26)$$

$$\left. \left. \frac{1}{\mu_o} (\nabla \times \nabla \times \mathbf{A}^T) \right) \right\} +$$

$$\frac{1}{\mu_o} \int_\Gamma d\theta dz \delta \mathbf{A} \left\{ r \frac{\partial \mathbf{A}^T}{\partial r} \right\}$$

Note that $\mathbf{A}^T = \{A_r, A_\theta, A_z\}$, which reduces to $\mathbf{A}^T = \{0, 0, A_z\}$ for the one-dimensional case and also that $d\Gamma = d\theta dz$. Constraining the value of $\mathbf{A} = 0$ at $r = R_{wire}$ causes both boundary terms in the previous variation to vanish. At $r = R_{wire}$, the value of $\mathbf{B}$ will be the same as the value for $\mathbf{B}$ given by a linear conductor with the *same* current flowing through it. This is a direct consequence of *Ampere's circuital law*, $\int_s \mathbf{B} \cdot ds = \mu I$. From $\nabla \times \mathbf{A} = \mathbf{B}$, the second boundary term becomes

$$\frac{1}{\mu_o} \int_\Gamma d\theta dz \delta \mathbf{A} \left\{ r_{wire} \mathbf{B} \right\} \quad (27)$$

Using *Ampere's law*, this becomes

$$\int_\Gamma d\theta dz \delta \mathbf{A} \left\{ \frac{I}{2\pi} \right\} \quad (28)$$

This will give a reaction force at $r = R_{wire}$ (after integrating over $d\Gamma$) of $-I$. The required boundary condition is that $A_z(r=0)$ is constrained to zero, but doing this will give a reaction force at $r = 0$ of $-I$. To maintain the same reaction force, a current I is added to the boundary at $r = 0$ and a current $-I$ is added at $r = R_{wire}$. This gives the residual (for $A_z(r=0) = 0$):

$$\int_V dV \left\{ \frac{1}{\mu_o} (\nabla \times \nabla \times \mathbf{A}) + \frac{q^* \hbar}{m^*} (\nabla \psi_R \psi_I - \nabla \psi_I \psi_R) + \frac{q^{*2}}{m^*} \mathbf{A} (\psi_R{}^2 + \psi_I{}^2) \right\} = 0 \quad (29)$$

From Maxwell's laws, it is known that $\mu_o^{-1} \nabla \times \nabla \times \mathbf{A} = \mathbf{J}$; substituting this formula into the above equation gives the constraint on $\mathbf{J}$, i.e.,

$$\int_V dV \left\{ \mathbf{J} + \frac{q^* \hbar}{m^*} (\nabla \psi_R \psi_I - \nabla \psi_I \psi_R) + \frac{q^{*2}}{m^*} \mathbf{A} (\psi_R{}^2 + \psi_I{}^2) \right\} = 0 \quad (30)$$

14

For one dimension, multiplying the above equation by the Lagrange multiplier λ_L and adding it, along with the current conservation constraint λ_g, to the Helmholtz free energy give the desired functional for a superconducting finite element. This topic and the mathematics will be taken up in a later section.

5.2 Evaluation of Material Parameters α and β †

Deep inside a superconductor, due to screening effects (the Meissner effect), there are no fields or gradients. The functional ΔF's last terms drop out and the resulting equation is

$$\Delta F = -\alpha|\psi|^2 + \tfrac{1}{2}\beta|\psi|^4 \tag{31}$$

Near the second order phase transition, at the critical temperature, the minimum value for the free energy occurs when

$$\frac{\partial \Delta F}{\partial \psi} = -2\alpha|\psi| + 2\beta|\psi|^3 = 0 \tag{32}$$

$$|\psi|^2 = |\psi_\infty|^2 = \frac{\alpha}{\beta} \tag{33}$$

where $|\psi_\infty|^2$ is the value for the number density of superconducting charge carriers deep within the conductor. Substituting $|\psi_\infty|^2$ back into the preceding equation for ΔF, gives

$$\Delta F = -\frac{\alpha^2}{\beta} + \frac{\alpha^2}{2\beta} = -\frac{\alpha^2}{2\beta} \tag{34}$$

When the critical field $\mathbf{B}_c$ is applied, $\Delta F = -\mathbf{B}_c^2/2\mu_o$. Because of this condition, deep inside a superconductor, where no gradients are present, the following approximation to ΔF can be made

$$\Delta F = -\frac{\mathbf{B}_c^2}{2\mu_o} = -\frac{\alpha^2}{2\beta} \Rightarrow \frac{\mathbf{B}_c^2}{\mu_o} = \frac{\alpha^2}{\beta} \tag{35}$$

The work, W, done in setting up a current distribution $\mathbf{J}$ [12] is

$$W = -\tfrac{1}{2} \int_V \mathbf{J}^T \mathbf{A} dV \tag{36}$$

From London theory [14, p. 84], with λ_{eff} equal to the effective London penetration depth, the following equation relating $\mathbf{J}$ and $\mathbf{A}$ is derived

---

† The following has been abstracted from Tinkham's textbook [14], pp. 105-109.

$$J = -\frac{1}{\mu_o \lambda_{eff}^2} A \tag{37}$$

Substitution of this expression for J into the equation for W gives the result

$$W = \frac{1}{2\mu_o \lambda_{eff}^2} \int_V A^T A \, dV \tag{38}$$

From Ginzberg-Landau theory [14, p. 107] , the expression for the work done in setting up a current density J is defined as being

$$W = \int_V \frac{q^{*2}}{2m^*} A^T A |\psi_\infty|^2 dV \tag{39}$$

If gradients of the order parameter are zero and there are no external fields present, both of the above equations are good approximations to W. Equating these two expressions for W gives

$$\frac{1}{2\mu_o \lambda_{eff}^2} = \frac{q^{*2}}{2m^*} |\psi_\infty|^2 \tag{40}$$

Algebraic manipulation produces

$$|\psi_\infty|^2 = \frac{m^*}{\mu_o q^{*2} \lambda_{eff}^2} = \frac{\alpha}{\beta} \tag{41}$$

Solving for β gives

$$\beta = \alpha \frac{\mu_o q^{*2} \lambda_{eff}^2}{m^*} \tag{42}$$

From before

$$\frac{B_c^2}{\mu_o} = \frac{\alpha^2}{\beta} \tag{43}$$

Substitution for β and more algebra produces the following values for α and β

$$\alpha = \frac{q^{*2}}{m^*} B_c^2 \lambda_{eff}^2$$
$$\beta = \frac{\mu_o q^{*4}}{m^{*2}} B_c^2 \lambda_{eff}^4 \tag{44}$$

Equating $|\psi_\infty|^2$ with n_s^*, which is the number of superconducting electron pairs, we see that to be consistent with London theory

$$
\begin{aligned}
q^* &= -2e &&= \text{twice the electron charge} \\
m^* &= 2m &&= \text{twice the electron mass}
\end{aligned}
$$

5.3 Analysis of the London Type Superconductor

The solution of the discretized superconductor follows the equilibrium curve for ΔF. This curve has at least one critical point, at $I = 0$. To make numerical experiments proceed, a good approximation to the solution vector is needed to move the solution off this point. The London type superconductor is such an approximation and is used in this work to advance the solution. For a London type superconductor, the gradient terms are assumed to be small, and $\psi_R{}^2 + \psi_I{}^2$ goes to $|\psi_\infty|^2$ over the whole conductor. Making these approximations to the previously derived Ginzburg-Landau equations produces

$$
\mathbf{J} = -\frac{q^{*2}}{m^*}\mathbf{A}|\psi_\infty|^2 \tag{45}
$$

Performing some algebra and vector mechanics gives us the differential equations for **B**

$$
\nabla \times \mathbf{J} = -\frac{q^{*2}}{m^*}\nabla \times \mathbf{A}|\psi_\infty|^2 \tag{46}
$$

$$
\frac{1}{\mu_o}\nabla \times (\nabla \times (\nabla \times \mathbf{A})) = -\frac{q^{*2}}{m^*}\nabla \times \mathbf{A}|\psi_\infty|^2 \tag{47}
$$

$$
\nabla \times (\nabla \times \mathbf{B}) \;=\; -\mu_o\frac{q^{*2}}{m^*}|\psi_\infty|^2\mathbf{B} \;=\; -\frac{1}{\lambda_{eff}^2}\mathbf{B} \tag{48}
$$

In one dimension, this becomes

$$
\frac{\partial^2 B_\theta}{\partial r^2} + \frac{1}{r}\frac{\partial B_\theta}{\partial r} - \left(\frac{1}{\lambda_{eff}^2} + \frac{1}{r^2}\right)B_\theta = 0 \tag{49}
$$

Letting $B_\theta/\lambda_{eff}^2 = U_\theta(r)$, $\nu^2 = 1$ and $r/\lambda_{eff} = x$ produces

$$
\frac{\partial^2 U_\theta(x)}{\partial x^2} + \frac{1}{x}\frac{\partial U_\theta(x)}{\partial x} - \left(1 + \frac{\nu^2}{x^2}\right)U_\theta(x) = 0 \tag{50}
$$

This is just the modified Bessel equation whose solution is $U_\theta(x) = a\mathcal{I}_\nu(x) + b\mathcal{K}_\nu(x)$. $\mathcal{I}_\nu$ and $\mathcal{K}_\nu$ are the modified Bessel functions, and a and b are constants dependent upon

17

the boundary conditions. For the solution to remain bounded as it approaches 0, $b = 0$, because $\mathcal{K}_\nu(x) \to \infty$ as $x \to 0$. Using this information, the solution becomes

$$U_\theta(x) = a\mathcal{I}_1(x) = U_\theta\left(\frac{r}{\lambda_{eff}}\right) = a\mathcal{I}_1\left(\frac{r}{\lambda_{eff}}\right) \tag{51}$$

$$B_\theta\left(\frac{r}{\lambda_{eff}}\right) = a\lambda_{eff}^2\mathcal{I}_1\left(\frac{r}{\lambda_{eff}}\right) \tag{52}$$

At $r = R_{wire}$, $B_\theta = \lambda\mu_o I_L/2\pi R_{wire}$. Substitution gives

$$a = \frac{\lambda\mu_o I_L}{2\pi R_{wire}\lambda_{eff}^2}\mathcal{I}_1^{-1}\left(\frac{R_{wire}}{\lambda_{eff}}\right) \tag{53}$$

Using the identity $\nabla \times \mathbf{A} = \mathbf{B}$, the relations $A_z(r/\lambda_{eff}) = -a\lambda_{eff}^3\mathcal{I}_0(r/\lambda_{eff})$, and $J_z = a\lambda_{eff}/\mu_o\mathcal{I}_0(r/\lambda_{eff})$ can be derived. The previous formula for $\mathbf{J}$ predicts the nodal or positional value of $\mathbf{J}$. The mean value for J_z is desired rather than this formula because any finite element developed in this work predicts the mean of $\mathbf{J}$ over an element. Using r_i and r_j to represent the inner and outermost nodal positions of an element, J_z is integrated over the volume of the element and divided by this volume to produce the mean value:

$$J_{mean}^e = \frac{\int J_z(x)\,x\,dx}{\int x\,dx} = 2a\frac{\lambda_{eff}}{\mu_o}\frac{\mathcal{I}_1(x)}{x}\bigg|_{x_i}^{x_j} = 2a\frac{\lambda_{eff}^2}{\mu_o}\frac{\mathcal{I}_1\left(\frac{r}{\lambda_{eff}}\right)}{r}\bigg|_{r_i/\lambda_{eff}}^{r_j/\lambda_{eff}} \tag{54}$$

5.4 One Dimensional Superconducting Finite Element

For the one-dimensional axisymmetric case, the discretized energy functional, minus the boundary terms of equation (26), is expressed as

$$
\begin{aligned}
U = \sum_{n=1}^{numel} \int_{V_m^e} dV_m^e \Big\{ &-\alpha(\psi_{I_n}^T \mathbf{N}_n^T \mathbf{N}_n \psi_{I_n} + \psi_{R_n}^T \mathbf{N}_n^T \mathbf{N}_n \psi_{R_n}) \\
&+ \tfrac{1}{2}\beta(\psi_{I_n}^T \mathbf{N}_n^T \mathbf{N}_n \psi_{I_n} + \psi_{R_n}^T \mathbf{N}_n^T \mathbf{N}_n \psi_{R_n})^2 \\
&+ \frac{1}{2m_*}\Big[\hbar^2(\psi_{I_n}^T \nabla \mathbf{N}_n^T \nabla \mathbf{N}_n \psi_{I_n} + \psi_{R_n}^T \nabla \mathbf{N}_n^T \nabla \mathbf{N}_n \psi_{R_n}) \\
&+ 2q^*\hbar \mathbf{A}_n^T \mathbf{N}_n^T(\psi_{R_n}^T \nabla \mathbf{N}_n^T \mathbf{N}_n \psi_{I_n} - \psi_{I_n}^T \nabla \mathbf{N}_n^T \mathbf{N}_n \psi_{R_n}) \\
&+ q^{*2}\mathbf{A}_n^T \mathbf{N}_n^T \mathbf{N}_n \mathbf{A}_n(\psi_{I_n}^T \mathbf{N}_n^T \mathbf{N}_n \psi_{I_n} + \psi_{R_n}^T \mathbf{N}_n^T \mathbf{N}_n \psi_{R_n})\Big] \\
&+ \lambda_{L_n}^e \Big[\frac{q^*\hbar}{m^*}(\psi_{R_n}^T \nabla \mathbf{N}_n^T \mathbf{N}_n \psi_{I_n} - \psi_{I_n}^T \nabla \mathbf{N}_n^T \mathbf{N}_n \psi_{R_n}) \\
&+ \frac{q^{*2}}{m^*}\mathbf{A}_n^T \mathbf{N}_n^T(\psi_{I_n}^T \mathbf{N}_n^T \mathbf{N}_n \psi_{I_n} + \psi_{R_n}^T \mathbf{N}_n^T \mathbf{N}_n \psi_{R_n}) + \mathbf{J}\Big] \\
&+ \frac{1}{2\mu_o}(\nabla \times \mathbf{N}_n \mathbf{A}_n)^T(\nabla \times \mathbf{N}_n \mathbf{A}_n) \\
&+ \lambda_g \Big\{I_o + \lambda I_L - \sum_{n=1}^{numel} \int_{\Gamma_n^e} d\Gamma_n^e \mathbf{J}_n \Big\}
\end{aligned}
\tag{55}
$$

Variation of the above with respect to ψ_R produces the following residuals on an elemental level

$$
\begin{aligned}
\mathbf{r}_{\psi_R^e} = \int_{V^e} dV^e \delta\psi_R^{eT} \Big\{ &-\alpha \mathbf{N}^T \mathbf{N}\psi_R^e + 2\beta \mathbf{N}^T(\psi_I^{eT}\mathbf{N}^T\mathbf{N}\psi_I^e + \psi_R^{eT}\mathbf{N}^T\mathbf{N}\psi_R^e)\mathbf{N}\psi_R^e + \\
&\frac{1}{m^*}\big[\hbar^2 \nabla\mathbf{N}^T\nabla\mathbf{N}\psi_R^e + q^*\hbar(\nabla\mathbf{N}^T\mathbf{N}\psi_I^e - \mathbf{N}\nabla\mathbf{N}\psi_I^e)\mathbf{N}\mathbf{A}^e + \\
&q^{*2}\mathbf{N}^T\mathbf{N}\psi_R^e(\mathbf{A}^{eT}\mathbf{N}^T\mathbf{N}\mathbf{A}^e)\big] + \\
&\lambda_L^e\big[\frac{q^*\hbar}{m^*}(\nabla\mathbf{N}^T\mathbf{N}\psi_I^e - \mathbf{N}^T\nabla\mathbf{N}\psi_I^e) + 2\frac{q^{*2}}{m^*}\mathbf{N}^T\mathbf{N}\psi_R^e\mathbf{A}^e\big] \Big\}
\end{aligned}
\tag{56}
$$

For ψ_I, we get

$$\mathbf{r}_{\psi_I^\epsilon} = \int_{V^\epsilon} dV^\epsilon \delta\psi_I^{\epsilon T} \Big\{ -\alpha \mathbf{N}^T \mathbf{N} \psi_I^\epsilon + 2\beta \mathbf{N}^T (\psi_I^{\epsilon T} \mathbf{N}^T \mathbf{N} \psi_I^\epsilon + \psi_R^{\epsilon T} \mathbf{N}^T \mathbf{N} \psi_R^\epsilon) \mathbf{N} \psi_I^\epsilon +$$

$$\frac{1}{m^*} [\hbar^2 \nabla \mathbf{N}^T \nabla \mathbf{N} \psi_I^\epsilon - q^* \hbar (\nabla \mathbf{N}^T \mathbf{N} \psi_R^\epsilon - \mathbf{N} \nabla \mathbf{N} \psi_R^\epsilon) \mathbf{N} \mathbf{A}^\epsilon +$$

$$q^{*2} \mathbf{N}^T \mathbf{N} \psi_I^\epsilon (\mathbf{A}^{\epsilon T} \mathbf{N}^T \mathbf{N} \mathbf{A}^\epsilon)] +$$

$$\lambda_L^\epsilon [-\frac{q^* \hbar}{m^*} (\nabla \mathbf{N}^T \mathbf{N} \psi_R^\epsilon - \mathbf{N}^T \nabla \mathbf{N} \psi_R^\epsilon) + 2\frac{q^{*2}}{m^*} \mathbf{N}^T \mathbf{N} \psi_I^\epsilon \mathbf{A}^\epsilon] \Big\} \tag{57}$$

For $\mathbf{A}$ we get

$$\mathbf{r}_{\mathbf{A}^\epsilon} = \int_{V^\epsilon} dV^\epsilon \delta \mathbf{A}^{\epsilon T} \Big\{ \mathbf{N}^T (\psi_R^{\epsilon T} \nabla \mathbf{N}^T \mathbf{N} \psi_I^\epsilon - \psi_I^{\epsilon T} \nabla \mathbf{N}^T \mathbf{N} \psi_R^\epsilon) \frac{q^* \hbar}{m^*} +$$

$$\frac{q^{*2}}{m^*} \mathbf{N}^T \mathbf{N} \mathbf{A}^\epsilon (\psi_I^{\epsilon T} \mathbf{N}^T \mathbf{N} \psi_I^\epsilon + \psi_R^{\epsilon T} \mathbf{N}^T \mathbf{N} \psi_R^\epsilon) +$$

$$\mu_o^{-1} \nabla \mathbf{N}^T \nabla \mathbf{N} \mathbf{A}^\epsilon + \lambda_L^\epsilon \mathbf{N}^T (\frac{q^{*2}}{m^*} (\psi_I^{\epsilon T} \mathbf{N}^T \mathbf{N} \psi_I^\epsilon + \psi_R^{\epsilon T} \mathbf{N}^T \mathbf{N} \psi_R^\epsilon)) \Big\} \tag{58}$$

For variation with respect to the $\mathbf{J}_i^\epsilon$'s, we get

$$\mathbf{r}_{\mathbf{J}^\epsilon} = \int_{V^\epsilon} dV^\epsilon \delta \mathbf{J}^\epsilon \lambda_L^\epsilon - \int_{\Gamma^\epsilon} d\Gamma^\epsilon \delta \mathbf{J}^\epsilon \lambda_g \tag{59}$$

Variation of the λ_L^ϵ's gives

$$\mathbf{r}_{\lambda_L^\epsilon} = \int_{V^\epsilon} dV^\epsilon \delta \lambda_L^\epsilon \Big\{ \frac{q^* \hbar}{m^*} (\psi_R^{\epsilon T} \nabla \mathbf{N}^T \mathbf{N} \psi_I^\epsilon - \psi_I^{\epsilon T} \nabla \mathbf{N}^T \mathbf{N} \psi_R^\epsilon) +$$

$$\frac{q^{*2}}{m^*} (\psi_R^{\epsilon T} \mathbf{N}^T \mathbf{N} \psi_R^\epsilon + \psi_I^{\epsilon T} \mathbf{N}^T \mathbf{N} \psi_I^\epsilon) \mathbf{N} \mathbf{A}^\epsilon + \mathbf{J}^\epsilon +$$

$$\int_\Gamma d\theta dz \frac{I_o + \lambda I_L}{2\pi} \Big\} \tag{60}$$

And the variation of λ_g (for an *element*) produces

$$\delta \lambda_g \Big(\frac{I_o + \lambda I_L}{numel} - \int_{\Gamma^\epsilon} d\Gamma^\epsilon \mathbf{J}^\epsilon \Big) \tag{61}$$

Making the substitutions

$$\Psi_I^e = N\psi_I^e \qquad \frac{\partial \Psi_I^e}{\partial r} = \nabla \psi_I^e$$

$$\Psi_R^e = N\psi_R^e \qquad \frac{\partial \Psi_R^e}{\partial r} = \nabla \psi_R^e$$

$$\mathcal{A}^e = N\mathbf{A}^e \qquad \frac{\partial \mathcal{A}^e}{\partial r} = \nabla \mathbf{A}^e$$

gives for the internal force vector

$$\mathbf{f}^e = \begin{Bmatrix} \mathbf{f}_{\psi_R^e} \\ \mathbf{f}_{\psi_I^e} \\ \mathbf{f}_{\mathbf{A}^e} \\ \mathbf{f}_{\lambda_L^e} \\ \mathbf{f}_{\mathbf{J}^e} \\ \mathbf{f}_{\lambda_g} \end{Bmatrix} \tag{62}$$

where

$$\mathbf{f}_{\psi_R^e} = \int_{V^e} dV^e \Big\{ N^T \big(2\Psi_R^e(-\alpha + \beta(\Psi_I^{e2} + \Psi_R^{e2}))\big) - \frac{q^*\hbar}{m^*}\frac{\partial \Psi_I^e}{\partial r}(\mathcal{A}^e + \lambda_L^e) +$$

$$\frac{q^{*2}}{m^*}\mathcal{A}^e\Psi_R^e(\mathcal{A}^e + 2\lambda_L^e)\big) + \nabla N^T\big(\frac{\hbar^2}{m^*}\frac{\partial \Psi_R^e}{\partial r} + \frac{q^*\hbar}{m^*}\Psi_I^e(\mathcal{A}^e + \lambda_L^e)\big)\Big\} \tag{63}$$

$$\mathbf{f}_{\psi_I^e} = \int_{V^e} dV^e \Big\{ N^T \big(2\Psi_I^e(-\alpha + \beta(\Psi_I^{e2} + \Psi_R^{e2}))\big) + \frac{q^*\hbar}{m^*}\frac{\partial \Psi_R^e}{\partial r}(\mathcal{A}^e + \lambda_L^e) +$$

$$\frac{q^{*2}}{m^*}\mathcal{A}^e\Psi_I^e(\mathcal{A}^e + 2\lambda_L^e)\big) + \nabla N^T\big(\frac{\hbar^2}{m^*}\frac{\partial \Psi_I^e}{\partial r} - \frac{q^*\hbar}{m^*}\Psi_R^e(\mathcal{A}^e + \lambda_L^e)\big)\Big\} \tag{64}$$

$$\mathbf{f}_{\mathbf{A}^e} = \int_{V^e} dV^e \Big\{ N^T\big(\frac{q^*\hbar}{m^*}\big(\frac{\partial \Psi_R^e}{\partial r}\Psi_I^e - \frac{\partial \Psi_I^e}{\partial r}\Psi_R^e\big) + \frac{q^{*2}}{m^*}(\Psi_I^{e2} + \Psi_R^{e2})(\mathcal{A}^e + \lambda_L^e)\big) + \nabla N^T\frac{\partial \mathcal{A}^e}{\partial r}\mu_o^{-1}\Big\} \tag{65}$$

$$\mathbf{f}_{\mathbf{J}^e} = \int_{V^e} dV^e \lambda_L^e - \int_{\Gamma^e} d\Gamma^e \lambda_g \tag{66}$$

$$\mathbf{f}_{\lambda_L^e} = \int_{V^e} dV^e \Big\{ \frac{\hbar^2}{m^*}\big(\frac{\partial \Psi_R^e}{\partial r}\Psi_I^e - \frac{\partial \Psi_I^e}{\partial r}\Psi_R^e\big) + \frac{q^{*2}}{m^*}(\Psi_I^{e2} + prs^2)\mathcal{A}^e + \mathbf{J}^e + \int_{\Gamma} d\theta dz \frac{I_o}{2\pi} \Big\} \tag{67}$$

$$\mathbf{f}_{\lambda_g} = \frac{I_o}{numel} - \int_{\Gamma^e} d\Gamma^e \mathbf{J}^e \tag{68}$$

21

The loading vector **q** is

$$-\frac{\partial \mathbf{r}}{\partial \lambda} = -\int_\Gamma d\Gamma \frac{I_L}{2\pi} \begin{Bmatrix} -1 \\ 0 \\ \vdots \\ 0 \\ 1 \\ 0 \\ \vdots \\ 0 \\ 1 \end{Bmatrix} \tag{69}$$

Taking the second variation with respect to the $\mathbf{v}_i$'s produces the tangent stiffness matrix

$$\frac{\partial^2 U}{\partial \mathbf{A}^e \partial \mathbf{A}^e} = \int_{V^e} dV^e \delta \mathbf{A}^{eT} \left\{ \frac{q^{*2}}{m^*} \mathbf{N}^T \mathbf{N} (\psi_I^{eT} \mathbf{N}^T \mathbf{N} \psi_I^e + \psi_R^{eT} \mathbf{N}^T \mathbf{N} \psi_R^e) + \mu_o^{-1} \nabla \mathbf{N}^T \nabla \mathbf{N} \right\} \delta \mathbf{A}^e \tag{70}$$

$$\frac{\partial^2 U}{\partial \mathbf{A}^e \partial \psi_R^e} = \int_{V^e} dV^e \delta \mathbf{A}^{eT} \left\{ \mathbf{N}^T (\psi_I^{eT} \mathbf{N}^T \nabla \mathbf{N} - \psi_I^{eT} \nabla \mathbf{N}^T \mathbf{N}) \frac{q^* \hbar}{m^*} + \right.$$
$$\left. 2 \frac{q^{*2}}{m^*} \mathbf{N}^T (\mathbf{N} \mathbf{A}^e + \lambda_L^e)(\mathbf{N} \psi_R^e) \mathbf{N} \right\} \delta \psi_R^e \tag{71}$$

$$\frac{\partial^2 U}{\partial \mathbf{A}^e \partial \psi_I^e} = \int_{V^e} dV^e \delta \mathbf{A}^{eT} \left\{ \mathbf{N}^T (\psi_R^{eT} \nabla \mathbf{N}^T \mathbf{N} - \psi_R^{eT} \mathbf{N}^T \nabla \mathbf{N}) \frac{q^* \hbar}{m^*} + \right.$$
$$\left. 2 \frac{q^{*2}}{m^*} \mathbf{N}^T (\mathbf{N} \mathbf{A}^e + \lambda_L^e)(\mathbf{N} \psi_I^e) \mathbf{N} \right\} \delta \psi_I^e \tag{72}$$

$$\frac{\partial^2 U}{\partial \mathbf{A}^e \partial \lambda_L^e} = \int_{V^e} dV^e \delta \mathbf{A}^{eT} \left\{ \frac{q^{*2}}{m^*} \mathbf{N}^T (\psi_I^{eT} \mathbf{N}^T \mathbf{N} \psi_I^e + \psi_R^{eT} \mathbf{N}^T \mathbf{N} \psi_R^e) \right\} \delta \lambda_L^e \tag{73}$$

$$\frac{\partial^2 U}{\partial \mathbf{A}^e \partial \mathbf{J}^e} = 0 \tag{74}$$

$$\frac{\partial^2 U}{\partial \mathbf{A}^e \partial \lambda_g} = 0 \tag{75}$$

$$\frac{\partial^2 U}{\partial \psi^e_R \partial \psi^e_R} = \int_{V^e} dV^e \delta \psi^e_R{}^T \Big\{ \mathbf{N}^T \mathbf{N}(-2\alpha + 2\beta(\psi^e_I{}^T \mathbf{N}^T \mathbf{N} \psi^e_I + 3\psi^e_R{}^T \mathbf{N}^T \mathbf{N} \psi^e_R)) +$$

$$\frac{\hbar^2}{m^*} \nabla \mathbf{N}^T \nabla \mathbf{N} + \frac{q^{*2}}{m^*} \mathbf{N}^T \mathbf{N} (\mathbf{A}^e{}^T \mathbf{N}^T)(\mathbf{N} \mathbf{A}^e + 2\lambda^e_L) \Big\} \delta \psi^e_R \qquad (76)$$

$$\frac{\partial^2 U}{\partial \psi^e_R \partial \psi^e_I} = \int_{V^e} dV^e \delta \psi^e_R{}^T \Big\{ \mathbf{N}^T \mathbf{N} 4\beta(\psi^e_I{}^T \mathbf{N}^T \mathbf{N} \psi^e_R) + \frac{q^* \hbar}{m^*} (\mathbf{N} \mathbf{A}^e + \lambda^e_L)(\nabla^T \mathbf{N}^T \mathbf{N} - \mathbf{N}^T \nabla \mathbf{N}) \Big\} \delta \psi^e_I$$

$$(77)$$

$$\frac{\partial^2 U}{\partial \psi^e_R \partial \lambda^e_L} = \int_{V^e} dV^e \delta \psi^e_R{}^T \Big\{ \frac{q^* \hbar}{m^*} (\nabla \mathbf{N}^T \mathbf{N} \psi^e_I - \mathbf{N}^T \nabla \mathbf{N} \psi^e_I) + \mathbf{N}^T 2 \frac{q^{*2}}{m^*} \mathbf{N} \psi^e_R \mathbf{N} \mathbf{A}^e \Big\} \delta \lambda^e_L \quad (78)$$

$$\frac{\partial^2 U}{\partial \psi^e_R \partial \mathbf{J}^e} = 0 \qquad (79)$$

$$\frac{\partial^2 U}{\partial \psi^e_R \partial \lambda_g} = 0 \qquad (80)$$

$$\frac{\partial^2 U}{\partial \psi^e_I \partial \psi^e_I} = \int_{V^e} dV^e \delta \psi^e_I{}^T \Big\{ \mathbf{N}^T \mathbf{N}(-2\alpha + 2\beta(\psi^e_R{}^T \mathbf{N}^T \mathbf{N} \psi^e_R + 3\psi^e_I{}^T \mathbf{N}^T \mathbf{N} \psi^e_I)) +$$

$$\frac{\hbar^2}{m^*} \nabla \mathbf{N}^T \nabla \mathbf{N} + \frac{q^{*2}}{m^*} \mathbf{N}^T \mathbf{N} (\mathbf{A}^e{}^T \mathbf{N}^T)(\mathbf{N} \mathbf{A}^e + 2\lambda^e_L) \Big\} \delta \psi^e_I \qquad (81)$$

$$\frac{\partial^2 U}{\partial \psi^e_I \partial \lambda^e_L} = \int_{V^e} dV^e \delta \psi^e_I{}^T \Big\{ \frac{q^* \hbar}{m^*} (\mathbf{N}^T \nabla \mathbf{N} \psi^e_R - \nabla \mathbf{N}^T \mathbf{N} \psi^e_R) + \mathbf{N}^T 2 \frac{q^{*2}}{m^*} \mathbf{N} \psi^e_I \mathbf{N} \mathbf{A}^e \Big\} \delta \lambda^e_L \quad (82)$$

$$\frac{\partial^2 U}{\partial \psi^e_I \partial \mathbf{J}^e} = 0 \qquad (83)$$

$$\frac{\partial^2 U}{\partial \psi^e_I \partial \lambda_g} = 0 \qquad (84)$$

$$\frac{\partial^2 U}{\partial \lambda^e_L \partial \lambda^e_L} = 0 \qquad (85)$$

$$\frac{\partial^2 U}{\partial \lambda^e_L \partial \mathbf{J}^e} = \int_{V^e} dV^e \delta \lambda^e_L \delta \mathbf{J}^e \qquad (86)$$

23

$$\frac{\partial^2 U}{\partial \lambda_L^e \partial \lambda_g} = 0 \tag{87}$$

$$\frac{\partial^2 U}{\partial \mathbf{J}^e \partial \mathbf{J}^e} = 0 \tag{88}$$

$$\frac{\partial^2 U}{\partial \mathbf{J}^e \partial \lambda_g} = - \int_{\Gamma^e} d\Gamma^e \delta \mathbf{J}^e \delta \lambda_g \tag{89}$$

$$\frac{\partial^2 U}{\partial \lambda_g \partial \lambda_g} = 0 \tag{90}$$

Using the same notation as in the internal force vector $\mathbf{f}^e$, the tangent stiffness matrix may be represented as

$$
\mathbf{K}^e \mathbf{w}^e =
\begin{bmatrix}
\mathbf{K}_{\psi_R^e \psi_R^e} & \mathbf{K}_{\psi_R^e \psi_I^e} & \mathbf{K}_{\psi_R^e \mathbf{A}^e} & \mathbf{K}_{\psi_R^e \lambda_L^e} & \mathbf{0}_{2x1} & \mathbf{0}_{2x1} \\
 & \mathbf{K}_{\psi_I^e \psi_I^e} & \mathbf{K}_{\psi_I^e \mathbf{A}^e} & \mathbf{K}_{\psi_I^e \lambda_L^e} & \mathbf{0}_{2x1} & \mathbf{0}_{2x1} \\
 & & \mathbf{K}_{\mathbf{A}^e \mathbf{A}^e} & \mathbf{K}_{\mathbf{A}^e \lambda_L^e} & \mathbf{0}_{2x1} & \mathbf{0}_{2x1} \\
 & & & 0 & K_{\lambda_L^e \mathbf{J}^e} & 0 \\
 & symm. & & & 0 & K_{\lambda_g \mathbf{J}^e} \\
 & & & & & 0
\end{bmatrix}
\begin{Bmatrix}
\Delta \psi_R^e \\
\Delta \psi_I^e \\
\Delta \mathbf{A}^e \\
\Delta \lambda_L^e \\
\Delta \mathbf{J}^e \\
\Delta \lambda_g
\end{Bmatrix}
\tag{91}
$$

with

$$\mathbf{K}_{\psi_R^e \psi_R^e} =$$
$$\int_{V^e} dV^e \left\{ \mathbf{N}^T \left(-2\alpha + 2\beta \left(\Psi_I^{e\,2} + 3\Psi_R^{e\,2} \right) + \frac{q^{*2}}{m^*} \mathcal{A}^e \left(\mathcal{A}^e + 2\lambda_L^e \right) \right) \mathbf{N} + \frac{\hbar^2}{m^*} \nabla \mathbf{N}^T \nabla \mathbf{N} \right\} \tag{92}$$

$$\mathbf{K}_{\psi_R^e \psi_I^e} =$$
$$\int_{V^e} dV^e \left\{ \mathbf{N}^T \left(4\beta \Psi_I^e \Psi_R^e \right) \mathbf{N} + \frac{q^* \hbar}{m^*} \left(\mathcal{A}^e + \lambda_L^e \right) \left(\nabla \mathbf{N}^T \mathbf{N} - \mathbf{N}^T \nabla \mathbf{N} \right) \right\} \tag{93}$$

$$\mathbf{K}_{\psi_R^e \mathbf{A}^e} =$$
$$\int_{V^e} dV^e \left\{ \frac{q^* \hbar}{m^*} \left(\Psi_I^e \nabla \mathbf{N}^T \mathbf{N} - \frac{\partial \Psi_I^e}{\partial r} \mathbf{N}^T \mathbf{N} \right) + 2\frac{q^{*2}}{m^*} \left(\mathcal{A}^e + \lambda_L^e \right) \Psi_R^e \mathbf{N}^T \mathbf{N} \right\} \tag{94}$$

$$\mathbf{K}_{\psi_R^e \lambda_L^e} = \int_{V^e} dV^e \left\{ \frac{q^* \hbar}{m^*} \left(\nabla \mathbf{N}^T \Psi_I^e - \mathbf{N}^T \frac{\partial \Psi_I^e}{\partial r} \right) + \mathbf{N}^T \left(2\frac{q^{*2}}{m^*} \Psi_R^e \mathcal{A}^e \right) \right\} \tag{95}$$

$$\mathbf{K}_{\psi_I^e \psi_I^e} =$$

$$\int_{V^e} dV^e \left\{ \mathbf{N}^T \left(-2\alpha + 2\beta \left(\Psi_R^{e2} + 3\Psi_I^{e2} \right) + \frac{q^{*2}}{m^*} \mathcal{A}^e \left(\mathcal{A}^e + 2\lambda_L^e \right) \right) \mathbf{N} + \frac{\hbar^2}{m^*} \nabla \mathbf{N}^T \nabla \mathbf{N} \right\} \tag{96}$$

$$\mathbf{K}_{\psi_I^e \mathbf{A}^e} =$$

$$\int_{V^e} dV^e \left\{ \frac{q^* \hbar}{m^*} \left(\frac{\partial \Psi_R^e}{\partial r} \mathbf{N}^T \mathbf{N} - \Psi_R^e \nabla \mathbf{N}^T \mathbf{N} \right) + 2 \frac{q^{*2}}{m^*} \left(\mathcal{A}^e + \lambda_L^e \right) \Psi_I^e \mathbf{N}^T \mathbf{N} \right\} \tag{97}$$

$$\mathbf{K}_{\psi_I^e \lambda_L^e} = \int_{V^e} dV^e \left\{ \frac{q^* \hbar}{m^*} \left(\frac{\partial \Psi_R^e}{\partial r} \mathbf{N}^T - \Psi_R^e \nabla \mathbf{N}^T \right) + \mathbf{N}^T \left(2 \frac{q^{*2}}{m^*} \Psi_I^e \mathcal{A}^e \right) \right\} \tag{98}$$

$$\mathbf{K}_{\mathbf{A}^e \mathbf{A}^e} = \int_{V^e} dV^e \left\{ \frac{q^{*2}}{m^*} \mathbf{N}^T \mathbf{N} \left(\Psi_I^{e2} + \Psi_R^{e2} \right) + \frac{1}{\mu_o} \nabla \mathbf{N}^T \nabla \mathbf{N} \right\} \tag{99}$$

$$\mathbf{K}_{\mathbf{A}^e \lambda_L^e} = \int_{V^e} dV^e \left\{ \frac{q^{*2}}{m^*} \mathbf{N}^T \left(\Psi_I^{e2} + \Psi_R^{e2} \right) \right\} \tag{100}$$

$$K_{\lambda_L^e \mathbf{J}^e} = \int_{V^e} dV^e \tag{101}$$

$$K_{\mathbf{J}^e \lambda_g} = \int_{\Gamma^e} d\Gamma^e \tag{102}$$

6. NUMERICAL EXPERIMENTS

The finite element formulation described in the preceding section has been applied to the solution of a one-dimensional axisymmetric superconducting wire. This problem was treated with a bar-like element. Each element contains two end nodes, one centroidal node and a common global node as in the previously described linear element. These nodes are defined by their radial position r_j^e. Unlike the linear problem, this element contains three degrees of freedom on the two end nodes, namely ψ_{rj}, ψ_{ij}, and $\mathbf{A}_j$. Standard linear shape functions are used to interpolate these quantities across an element and provide the C^o continuity required by the variational formulation. The centroidal node carries no physical significance, and is used to provide the extra degrees of freedom for the elemental current densities and Lagrangian multipliers, λ_L^e and $\mathbf{J}^e$. The common global node is assigned the degree of freedom for λ_g. This gives each element a total of $2 \times 3 + 2 \times 1 + 1 = 9$ degrees of freedom.

For the calculation of the tangent stiffness, internal force vector and the loading vector, the permeability is a constant μ_o. The London penetration depth and intrinsic Pippard

25

coherence length for aluminum were used to calculate the critical magnetic field B_c and the effective London penetration depth λ_{eff} [13, p.337]. The subroutine that generates the elements in the coding, calculates the material parameters α and β, and assigns them to each superconducting element. The tangent stiffness matrix, internal force vector and external force vector are calculated by numerical quadrature using a 2 point Gauss formula.

6.1 Applying Boundary Conditions

The finite element mesh is terminated at R_T, as in the linear conductor. To ensure that no superconducting flux can cross the conductor's outer edge into free space, the degrees of freedom corresponding to $\mathbf{J}$, ψ_R and ψ_I between R_{wire} and R_T are set equal to zero. At $r = R_{wire}$, ψ_R and ψ_I are also set to zero. By setting these values to zero, the boundary terms in equations (24) and (25) are required to go to zero. This choice also ensures that no superconducting flux can cross either of the boundary surfaces. At $r = 0$, the value for $\mathbf{A}$ is also set equal to zero, as discussed in section 5.1. This choice for $\mathbf{A}$ requires that $|\psi|$ become constant as the inner boundary of a superconductor is approached.

6.2 Assembly and Solution

This section will present the assembly techniques and the solution method used on the test problem. Table 2 presents the nomenclature used for quantities of interest.

The tangent stiffness, internal force and loading vectors are assembled following standard finite element techniques. The tangent stiffness matrix $\mathbf{K}$, is stored using a symmetric skyline storage scheme, and then modified for boundary conditions.

Since this is a nonlinear problem, nonlinear techniques must be used to solve for the displacements of the variables $\mathbf{A}^e$, ψ_R^e, ψ_I^e, $\mathbf{J}^e$, λ_L^e, and λ_g. An incremental scheme is employed to advance the solution along the equilibrium curve by making a good approximaton to the exact solution. An iterative technique is then used to converge to the exact solution. The constraint used to limit the distance travelled along the equilibrium curve is arclength control, i.e., $|\Delta s_n| - l_n$, where Δs_n is the distance along the curve, and l_n is the length of the increment, an input variable. The formula implemented in our coding for arclength control is listed below in its scaled and unscaled forms. Also listed are the formulas for the vectors a and g. The superposed tilde represents a scaled quantity.

Unscaled Form

$$\Delta s_n = \frac{1}{f_n} \left| \mathbf{w}_n^T \Delta \mathbf{v}_n + \Delta \lambda_n \right| - l_n \tag{103}$$

$$\mathbf{a}^T = \mathbf{w}_n / f_n \qquad g = \frac{1}{f_n} \tag{104}$$

Table 2   Solution Nomenclature

Symbol	Quantities
$\mathbf{K}_n$	Master tangent stiffness matrix at increment n
$\mathbf{q}$	Loading vector
$\mathbf{r}_n$	Residual vector at increment n
$\mathbf{f}_n$	External force vector at increment n
$\mathbf{v}_n$	Solution vector at increment n
$\Delta\mathbf{v}_n$	$\mathbf{v}_{n+1} - \mathbf{v}_n$
λ_n	Control parameter ($\lambda=0$, zero load, $\lambda=1$, full load)
$\mathbf{w}$	Incremental velocity vector $= \mathbf{K}_n^{-1}\mathbf{q}$
l_n	Input arclength constraint
$|\Delta s|$	Distance along equilibrium path
$\tilde{f}_n$	$\sqrt{1 + \mathbf{w}^T\mathbf{w}}$
$\mathbf{S}$	Scaling matrix
c	Constraint equation
$\mathbf{a}$	$\partial c/\partial \mathbf{v}$
g	$\partial c/\partial \lambda$
$\mathbf{v}_n^k$	Solution vector at step n and iteration k
$\mathbf{d}$	$\mathbf{v}_n^{k+1} - \mathbf{v}_n^k$
λ_n^k	λ at step n and iteration k
η	$\lambda_n^{k+1} - \lambda_n^k$
$j_{fac}, a_{fac}, \ldots$	first scaling factor for $\mathbf{J}$, $\mathbf{A}$, etc.
$j_{scale}, a_{scale}, \ldots$	second scaling factor for $\mathbf{J}$, $\mathbf{A}$, etc.
$j_{homogeneous}, a_{homogeneous}, \ldots$	third scaling factor for $\mathbf{J}$, $\mathbf{A}$, etc.

Scaled Form

$$\Delta\tilde{s}_n = \frac{1}{\tilde{f}_n}\left|\tilde{\mathbf{w}}_n^T\Delta\tilde{\mathbf{v}}_n + \Delta\lambda_n\right| - l_n \tag{105}$$

$$\mathbf{a}^T = \tilde{\mathbf{w}}_n/\tilde{f}_n \qquad g = 1/\tilde{f}_n \tag{106}$$

$$\Delta\tilde{\mathbf{v}} = \mathbf{S}\Delta\mathbf{v}, \quad \tilde{\mathbf{q}} = \mathbf{S}^{-1}\mathbf{q}, \quad \tilde{\mathbf{K}} = \mathbf{S}^{-1}\mathbf{K}\mathbf{S}^{-1},$$

$$\tilde{\mathbf{w}} = \mathbf{S}\mathbf{w}, \quad \tilde{f} = \sqrt{1 + \mathbf{w}^T\mathbf{S}^2\mathbf{w}} = \sqrt{1 + \tilde{\mathbf{w}}^T\tilde{\mathbf{w}}} \tag{107}$$

A forward Euler integration scheme was used to predict $\Delta\mathbf{v}_n$, λ_{n+1}, and $\mathbf{v}_{n+1}$. Appropriate formulas are listed below.

$$\Delta\lambda_n = \lambda_{n+1} - \lambda_n = \frac{l_n}{f_n} sign(\mathbf{q}^T\mathbf{w}),$$

$$\Delta\mathbf{v}_n = \mathbf{K}_n^{-1}\mathbf{q}_n\Delta\lambda_n = \mathbf{w}_n\Delta\lambda_n \qquad (108)$$

$$\mathbf{v}_{n+1} = \mathbf{v}_n + \Delta\mathbf{v}_n$$

A conventional Newton-Raphson technique was implemented for the corrector. This gives the linear system

$$\begin{bmatrix} \mathbf{K} & -\mathbf{q} \\ \mathbf{a}^T & g \end{bmatrix} \begin{Bmatrix} \mathbf{d} \\ \eta \end{Bmatrix} = - \begin{Bmatrix} \mathbf{r} \\ c \end{Bmatrix} \qquad (109)$$

Since this augmented system is not symmetric, the two linear symmetric systems below are solved for instead

$$\mathbf{K}\mathbf{d}_r = -\mathbf{r} \quad \mathbf{K}\mathbf{d}_q = \mathbf{q} \qquad (110)$$

to get

$$\eta = -\frac{c + \mathbf{a}^T\mathbf{d}_r}{g + \mathbf{a}^T\mathbf{d}_q}, \quad \mathbf{d} = \mathbf{d}_r + \eta\mathbf{d}_q \qquad (111)$$

which will finally give

$$\mathbf{v}_n^{k+1} = \mathbf{v}_n^k + \mathbf{d}, \quad \lambda_n^{k+1} = \lambda_n^k + \eta \qquad (112)$$

We then iterated until the 2-norm was less than a given tolerance ϵ.

6.3 Field Recovery

The primary quantity of interest is not any of the variables in the solution vector, but the derived quantity $\mathbf{B}$. This quantity can be computed by using one of two methods. The first is to use the identity $\mathbf{B} = \nabla \times \mathbf{A}$. Discretization in one dimension produces

$$\mathbf{B}_\theta = -\frac{\partial\mathbf{N}}{\partial r}\mathbf{A}^e = \frac{\mathbf{A}_j - \mathbf{A}_i}{l^e} \qquad (113)$$

where $\mathbf{A}_j$ and $\mathbf{A}_i$ are the values for $\mathbf{A}$ at the outer and innermost nodes of the element respectively, and l^e is the element length.

The second method is to use *Ampere's law*. Discretization in one dimension gives

$$B = \frac{I_{enclosed}}{2\pi r_n}, \qquad I_{enclosed} = \pi \sum_{i=1}^{n-1} J_i^e (r_{i+1}^2 - r_i^2) \qquad (114)$$

where r_n is the position of the outermost node of the element on which B is being evaluated. The innermost and outermost nodes of elements that are interior to r_n are r_i and r_{i+1}, respectively.

The advantage to the second method is that it can be used to predict the B field at the end nodes of the elements. The first method merely computes the mean of the field over the element. In the test problem, both methods are used to compute the B field and compared.

6.4 Numerical Nightmares in Solution Method

Starting the Solution Process

At $\lambda = 0$, the tangent stiffness matrix is singular if $I_o = 0$. K has a rank deficiency of 1 at this critical point. The eigenvector has only one component at the degree of freedom corresponding to λ_g. Multiplying the eigenvector by q^T gives us a non-zero value and tells us that this is a limit point. To move off of the limit point, initially a random perturbation technique was employed. All of the components of w were perturbed randomly in an effort to move the solution off of the limit point. This technique is not recommended because there is no guarantee that the approximate solution will be close enough to the equilibrium curve to iterate back onto it. Another failing is that the solution may progress back to the limit point because the perturbation pushed the guessed solution below the limit point on the equilibrium path. For the test problem studied here, this method failed approximately eighty percent of the time.

Instead, to get off the limit point, first all of the Lagrangian multipliers are constrained to zero, and then the results are fed into the corrector. When the results are fed into the corrector, the multipliers no longer are constrained to zero. The coding then iterates to the exact solution.

If the solution proceeds toward another critical point, the analytical solution for a London (extreme type I) superconductor is inserted into v, and is allowed to iterate from that point towards the solution. The London solutions contain the modified Bessel functions $\mathcal{I}_0$ and $\mathcal{I}_1$. The values for $\mathcal{I}_0$ and $\mathcal{I}_1$ are calculated using polynomial expansions [18] that are accurate to approximately 10^{-7} and then inserted into the v vector of the calling program.

Scaling of Variables

The arclength constraint is particularly sensitive to inhomogeneous physical dimensions in v. The different variables in v in this problem all have different physical dimensions. To improve stability of the solution method and to reduce the condition number of the master tangent stiffness matrix, a scaling was done in three parts on the variables in v.

The first part consists of scaling the variables to have a homogeneous physical dimension. The second part consists of scaling the new variables to reduce the condition number on the tangent stiffness matrix. The second scaling is done because although the dimensions in $\mathbf{v}$ may be homogeneous, one variable may only move 10^{-6} units per incremental step while another may move 10^6 units. The third scaling is a homogeneous scaling of all of the variables. This scaling can be used to reduce the order of magnitude of f_n so that the Newton-Raphson iterations becomes more stable. The total scaling factor for each variable is then represented by

$$S_{variable} = \frac{variable_{fac} 10^{variable_{scale}}}{variable_{homogeneous}}, \tag{115}$$

for example,

$$S_J = \frac{j_{fac} 10^{j_{scale}}}{j_{homogeneous}} \tag{116}$$

In the first part of the scaling, $\mathbf{K}$ is given units of volume, and then $\mathbf{v}\mathbf{v}^T$ is scaled so that it has units of energy per unit volume. With L, M, T, and Q representing units of distance, mass, time and charge respectively, this means that $\mathbf{v}$ should have units of $M^{1/2}L^{1/2}/T$. This also means that $\mathbf{A}$ and λ_L^ϵ have units of ML/TQ, ψ_I and ψ_R have units of $1/L^{3/2}$, $\mathbf{J}$ has units of Q/TL^2, and λ_g has units of $M^{1/2}L^{1/2}/T$. For $\tilde{\mathbf{v}} = \mathbf{S}\mathbf{v}$, a_{fac} has units of $Q/M^{1/2}L^{1/2}$, j_{fac} has units of $M^{1/2}L^{5/2}/Q$, ψ_{fac} has units of $M^{1/2}L^2/T$, $\lambda_{L\,fac}^\epsilon$ has units of $Q/M^{1/2}L^{1/2}$, and $\lambda_{g\,fac}$ has units of $Q/M^{1/2}L^{3/2}$. In previous experiments with linear electromagnetic finite elements, it was found that scaling $\mathbf{A}$ by $\mu_o^{-1/2}$ gave the desired units and stability, so a_{fac} is set to $\mu_o^{-1/2}$. Using the London approximation to the Ginzberg-Landau equations gives $j_{fac} = |-\mu_o^{-1/2}\lambda_{eff}^2|$. Numerical experiments produced $q^* B_c \lambda_{eff} r_{mean}/m^{*1/2}$ as a reasonable scaling value for ψ_{fac}, with r_{mean} being the mean value of the lengths of all of the elements. The value of $\lambda_{L\,fac}^\epsilon$ is set to the same value as a_{fac} because in their unscaled forms $\mathbf{A}$ and λ_L^ϵ have the same physical dimensions. Finally $\lambda_{g\,fac}$ is set to $\mu_o^{-1/2} R_{wire}^{-1}$ as a result of numerical experiments.

The second part of the scaling is done by performing numerical experiments. Two different variables can be monitored to determine what the values for a_{scale}, j_{scale}, ψ_{scale}, $\lambda_{L\,scale}^\epsilon$, and $\lambda_{g\,scale}$ should be. If $\tilde{\mathbf{v}}$ is monitored, the value of $\lambda_{g\,scale}$ is changed until $\mathbf{v}$ at the degree of freedom corresponding to λ_g is of the order of magnitude of 10^0. Then j_{scale}, $\lambda_{L\,scale}^\epsilon$, a_{scale}, and ψ_{scale} are set *in this order*, by reducing, at the corresponding degree of freedom, the largest value of $\tilde{\mathbf{v}}$ to an order of magnitude of 10^0.

The second variable that can be monitored is $1/d_{ii}$, where d_{ii} is the value of the ith element in the $\mathbf{D}$ matrix from the $\mathbf{L}^T\mathbf{D}\mathbf{L}$ decomposition of the master tangent stiffness matrix. In this scheme, the largest value of d_{ii}, for the degrees of freedom corresponding to ψ is reduced to an order of magnitude of 10^0 by adjusting ψ_{scale}. Then a_{scale}, $\lambda_{L\,scale}^\epsilon$, and j_{scale} are adjusted in the same manner. Finally $\lambda_{g\,scale}$ is adjusted in the same manner,

but then more numerical experiments are performed by adjusting it up and down one unit. While it is adjusted up and down, the condition number of the matrix is monitored. The direction which produces the lower condition number is chosen, and $\lambda_g scale$ is adjusted until the lowest condition number is achieved. For the numerical experiments performed here, the condition number was estimated by using a random perturbation technique.

No matter which variable is chosen, d_{ii} or $\tilde{v}$, sometimes these methods fail because K becomes singular. They usually fail because of a bad value for $\lambda^{\epsilon}_{L scale}$. If this happens it is recommended that the same procedures are followed, but get as close to reducing values to an order of 10^0 as possible. The last scaling value that produces a non-singular K is the one that should be used. It is recommended that the values for ψ_{scale}, $\lambda_{g scale}$, a_{scale}, $\lambda^{\epsilon}_{L scale}$, and j_{scale} be variables that are interactive input because sometimes many numerical experiments must be performed to achieve the best results. It is also recommended that the coding be set up such that when any of the second scaling factors are incremented one positive unit, the corresponding degrees of freedom in $\tilde{v}$ are scaled down by a power of 10, e.g., 10^{10} becomes 10^0 when 10 is the input scaling factor. This helps to eliminate confusion as to what the input scaling factor should be. If the variable d_{ii} is monitored, the d_{ii}'s that correspond to the degrees of freedom for ψ and A will be scaled in a similar manner, but the remaining degrees of freedom will move by a power of 10^2 when the scaling factor is incremented one positive unit, e.g., 10^{10} becomes 10^0 when 5 is input as a scaling factor. Both of these options have been implemented in the coding for the test problem presented here.

The third and final scaling factor is set by monitoring f_n. The idea here is to reduce f_n to an order of approximately one, as can be seen from equation (108). Unfortunately, sometimes doing this can raise the system's conditon number to an unacceptable value. This factor should only be used to reduce a system's condition number or to stabilize an already unstable solution process.

6.5 Test Problem

For our test problem, we use a finite element mesh similar to the one described in the section on linear conductors. The big difference between this problem and a linear conductor problem is that the charge carriers act like a fluid flow in a pipe with resistance. Most of the interesting physics occurs in a thin boundary type layer at the conductor/free space interface. Because of this phenomena, we generate a regular mesh of N_{bulk} elements in the interior of the conductor, and a geometric mesh of $N_{boundary}$ elements in the boundary layer. The mesh ratio, N_{bulk}, and $N_{boundary}$ are input values. Because the element for a free space magnetic field has been validated many times before, no elements were generated external to the conductor.

The leading term for the London solutions to J, A, and B is $\exp(x_j - x_{wire})$. Using this information, the depth of the boundary layer has been set to $5. \times 575. \times \lambda_{eff}$. This value was chosen for the boundary layer depth because it can be determined where the value for $\exp(x_j - x_{wire})$, where x_j is between $x_{boundary}$ and x_{wire}, is no less than 10^{-250}. The

choice of 10^{-250} ensures that machine underflows do not occur if the London solutions are calculated to move off of a critical point. Setting the boundary depth to $575. \times \lambda_{eff}$ does not allow the London solutions to go beyond machine precision over the whole boundary layer, but does increase the condition number on the tangent stiffness matrix. Numerical experiments showed that setting the boundary layer to five times this depth reduced the tangent stiffness condition number considerably.

The values of -12, -3, -5 -15, and -13 were chosen for a_{scale}, ψ_{scale}, j_{scale}, $\lambda_{L\ scale}$, and $\lambda_{g\ scale}$ respectively. These values were chosen by monitoring $\tilde{v}$ and adjusting the appropriate scaling factor as described in the previous subsection. The value for the third scaling factor was 10^6 and was chosen by monitoring the value for f_n and the tangent stiffness condition estimate.

All graphs presented here are for $\lambda = .00103$ with a tangent stiffness condition estimate of approximately 4×10^6. Figures 8 and 9 display the results for $|\psi|^2$ normalized by $|\psi_\infty^2|$. Figure 8 shows the behavior for $|\psi_{normalized}^2|$ over the whole mesh and Figure 9 the behavior in the boundary layer. Since aluminum is a Type I superconductor, these results match very well with expected physical behavior. The boundary conditions are seen to match well in that at both boundaries the slope for $|\psi_{normalized}|^2$ approaches zero (see equations 24,25).

Results for J are displayed in Figures 10 and 11. Figure 10 shows the behavior for J over the mesh, and Figure 11 the behavior in the boundary layer. The effects of the high condition number become apparent in Figure 11. Although the general behavior as exhibited in Figure 10 physically follows that of a Type I superconductor, inside the boundary layer J jumps up and down instead of increasing exponentially. The reason for the high condition number also becomes apparent. For Type I and II superconductors, B is excluded from the better part of the conductor. To match this physical situation, A and J must become zero for values of r between the center of the conductor and the boundary layer. The degrees of freedom in this region for A and J in the finite element formulation become approximately equal to zero and cause the condition number for the tangent stiffness matrix to rise.

The results for the B field are shown in Figures 12 and 13. The two different methods for calculating B as discussed in section 6.3 are displayed. Again Figure 12 shows behavior over the whole mesh, while Figure 13 shows behavior over the boundary layer. Surprisingly, in view of the high condition number, the finite difference method yields reasonable values for the mean value of B. The values of B calculated by using *Ampere's Circuital Law* do not perform well because the values for J are not accurate.

The finite element model also produced results for A, but these results are not presented here because the quantities of primary interest in this application are $|\psi|^2$, J and B.

7. CONCLUSIONS AND FUTURE WORK

The results obtained with the one-dimensional superconducting element are encouraging. Although the values obtained for **J** were not very good, the model performed well ehough to give us reasonable physical answers for **B**, **A** and $|\psi|^2$. They show that the variational formulation can provide good results for electromagnetic quantities inside a superconductor. The main difficulty is to reduce the tangent stiffness condition number so that reasonable values for **J** may be obtained: A reformulation of the terms involving **A** and **J** is suggested, since these terms go to zero over the majority of the model. A way to do this is to express **B** as the sum of an equivalent linear magnetic field, and the magnetic field due to the material nonlinearities (the magnetization field μ_o**M**). This gives the following equation for the last term of equation 22

$$\frac{1}{2\mu_o}(\nabla \times \mathbf{A} + \mathbf{B}_{applied})^T(\nabla \times \mathbf{A} + \mathbf{B}_{applied}) \tag{117}$$

where $\nabla \times \mathbf{A}$ now is equal to $\mu_o\mathbf{M}$. **J** is similarly split into $\mathbf{J}_{applied}$ and $\mathbf{J}_{material}$. This formulation should help to alleviate most of the conditioning problem because for the bulk of the conductor, $\mathbf{J}_{applied} = -\mathbf{J}_{material}$ and $\mathbf{A}_{applied} = -\mathbf{A}_{material}$. The solution that will be sought over this area, instead of being zero, will be just the negative of the linear solution. Any further conditioning problems will be addressed with any of the previous scaling techniques, or a diagonal scaling (Jacobi preconditioner) will be applied.

After the conditioning problem has been solved, the next step in the development of this element will be to add thermocoupling effects. Good semi-analytical approximations that relate temperature change to $\mathbf{B}_c$ and λ_{eff} are found in Tinkham[14]. These two variables, and their temperature dependence, directly effect the material parameters α and β. This temperature dependency will be added to the current coding along with an expression for the energy change due to temperature variation. If time permits, the final step in this research will be to extend the current formulation to two dimensions. The problem that will be studied will be a one dimensional infinite superconductor whose critical current has been exceeded. The superconducting flux varies in the radial and axial directions. Although finite difference formulations of this problem have yielded good results, none of them have been able to adequately match experimental data. The suspected problem has been that these formulations do not capture effects due to Joule heating of the wire. A two-dimensional superconducting element with thermal degrees of freedom appears to be the perfect vehicle to test that hypothesis.

Acknowledgements

References

1. FELIPPA, C. A. and T. L. GEERS, "Partitioned analysis of coupled mechanical systems," *Engineering Computations*, 5, 1988, pp. 123-133

2. PARK, K. C. and C. A. FELIPPA, "Partitioned analysis of coupled systems," Chapter 3 in *Computational Methods for Transient Analysis*, ed. by T. Belytschko and T. J. R. Hughes, North-Holland, Amsterdam–New York, 1983

3. FELIPPA, C. A.,, "The extended free formulation of finite elements in linear elasticity," *Journal of Applied Mechanics*, 56, 3, 1989, pp. 609-616

4. FELIPPA, C. A. and C. MILITELLO, "Developments in variational methods for high-performance plate and shell elements," in *Analytical and Computational Models for Shells*, CED Vol. 3, ed. by A. K. Noor, T. Belytschko and J. C. Simo, The American Society of Mechanical Engineers, ASME, New York, 1989, pp. 191-216

5. FELIPPA, C. A. and C. MILITELLO, "The variational formulation of high-performance finite elements: parametrized variational principles," (with C. Militello), *Computers & Structures*, 36, 1990, pp. 1-11

6. MILITELLO, C. and C. A. FELIPPA, "A variational justification of the assumed natural strain formulation of finite elements: I. Variational principles," (with C. Militello), *Computers & Structures*, 34, 1990, pp. 431-438

7. MILITELLO, C. and C. A. FELIPPA, "A variational justification of the assumed natural strain formulation of finite elements: II. The C^0 4-node plate element," *Computers & Structures*, 34, 1990, pp. 439-444

8. DAVIES, J. B., "The finite element method," Chapter 2 in *Numerical Techniques for Microwave and Millimeter-Wave Passive Structures*, ed. by T. Itoh, Wiley, New York, 1989

9. TROWBRIDGE, C. W., "Numerical solution of electromagnetic field problems in two and three dimensions," Chapter 18 in *Numerical Methods in Coupled Problems*, ed. by R. Lewis *et.al.*, Wiley, London, 1984

10. FELIPPA, C. A. and R. OHAYON, "Treatment of coupled fluid-structure interaction problems by a mixed variational principle," *Proceedings 7th International Conference on Finite*

Element Methods in Fluids, ed. by T. J. Chung *et.al.*, University of Alabama Press, Huntsville, Alabama, April 1989, pp. 555-563

11. FELIPPA, C. A. and R. OHAYON, "Mixed variational formulation of finite element analysis of acousto-elastic fluid-structure interaction," in *Journal of Fluids & Structures*, 4, 1990, pp. 35-57

12. EYGES, L., *The Classical Electromagnetic Field*, Dover, New York, 1980, pp.172-174

13. KITTEL, C., *Introduction to Solid State Physics*, 6th. ed, Wiley, New York, 1986

14. TINKHAM, M., *Introduction to Superconductivity*, Krieger Pub. Co., Malabar, Florida, 1975

15. SCHULER, J., and FELIPPA, C., " Electromagnetic Finite Elements Based On A Four-Potential Variational Principle", *Finite Elements in Analysis and Design*, 6, 1990, pp. 321-329

16. SCHULER, J., and FELIPPA, C., "Electromagnetic Axisymmetric Finite Elements Based on a Gauged Four-Potential Variational Principle", *Computing Systems in Engineering*, 1990, 1, pp. 273-284

17. YOURGRAU, W., and MANDELSTAM, S., *Variational Principles in Dynamics and Quantum Theory*, Dover Publications, Inc., New York, 1968, p.158, eqn. 309

18. PRESS, W., FLANNERY, B., TEUKOLSKY, S., and VETTERLING, W., *Numerical Recipes—The Art of Scientific Computing (Fortran Version)*, Cambridge University Press, Cambridge, England, 1990, pp.176-180
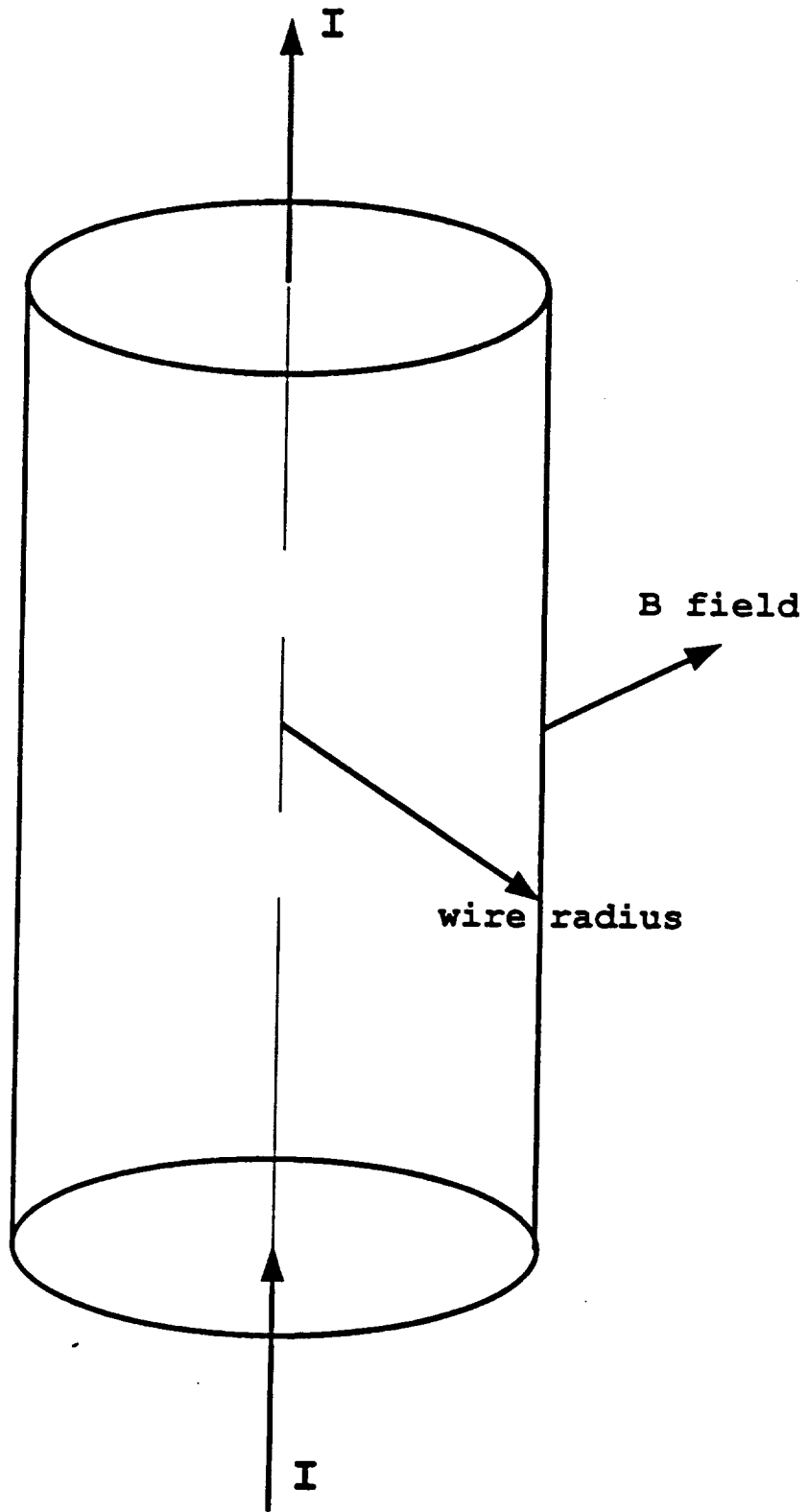
Figure 1. One dimensional infinite conductor
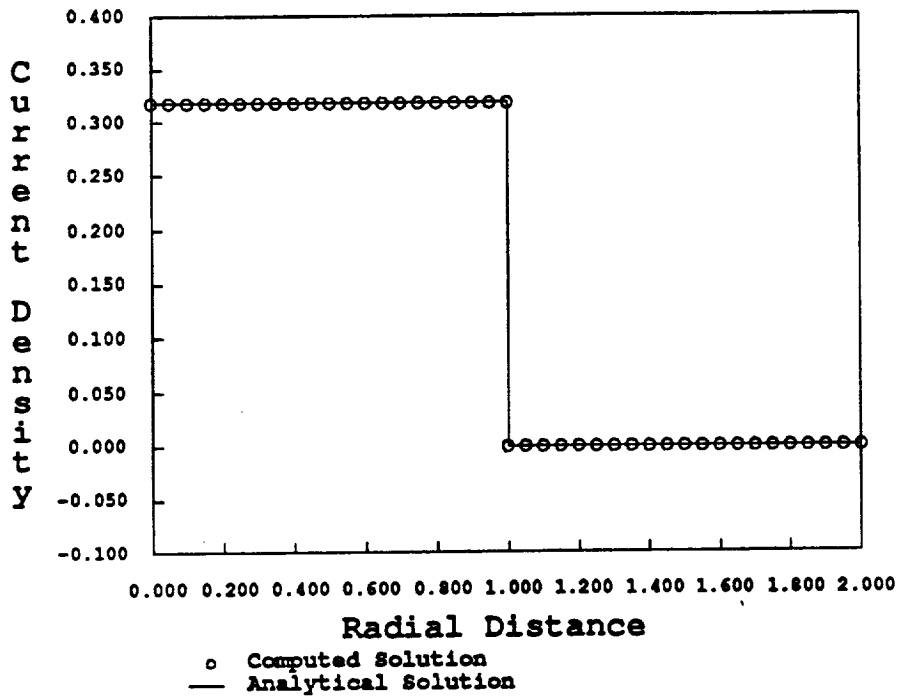
Figure 2.
J vs. radial distance, all elements equal conductivities. Computed
solution plotted as points to highlight accuracy of method in matching exact solution.
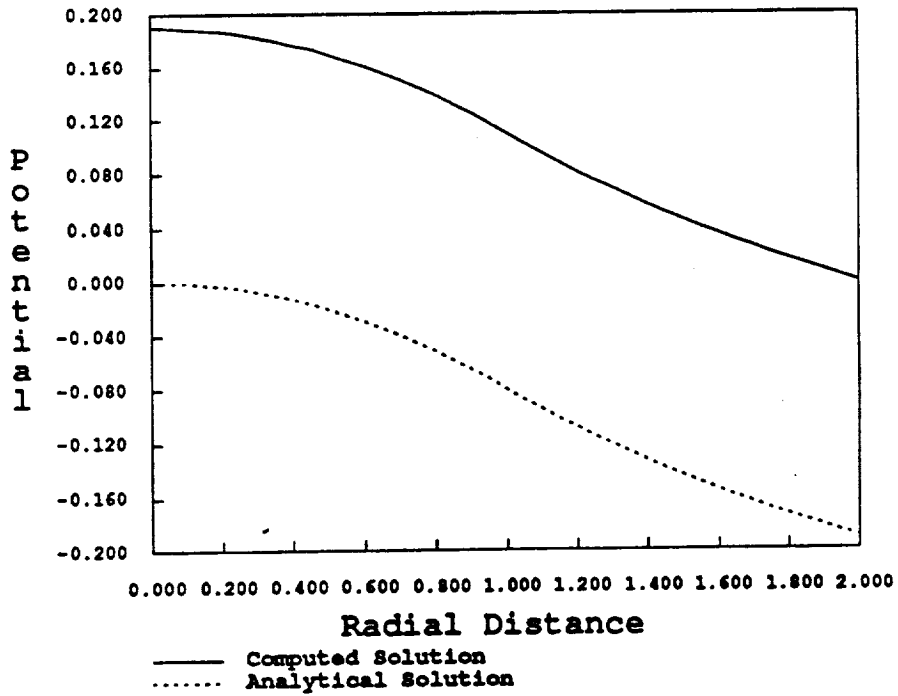
Figure 3.
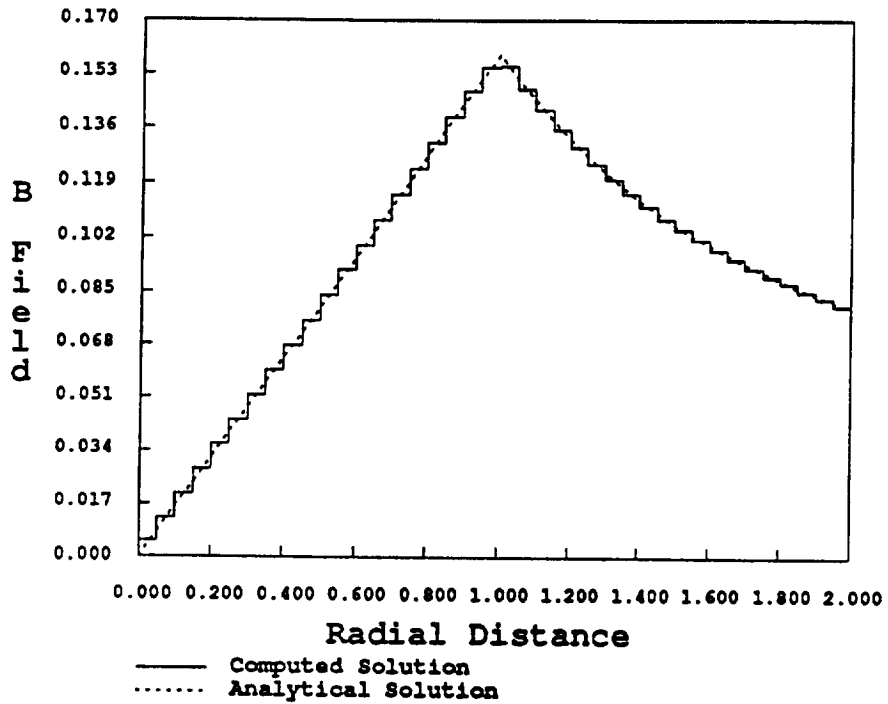A vs. radial distance, all elements equal conductivities.

Figure 4.
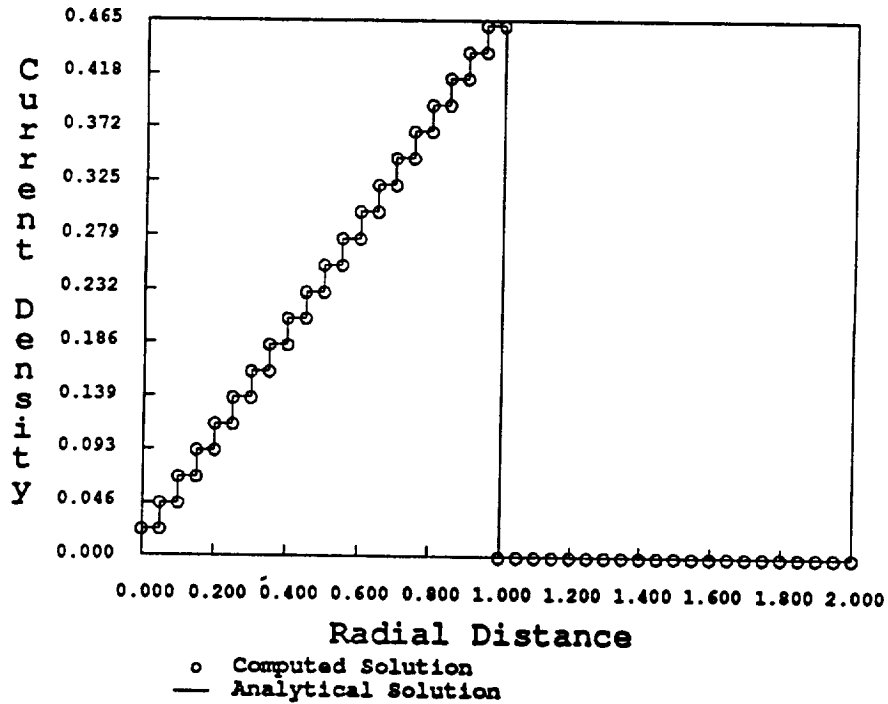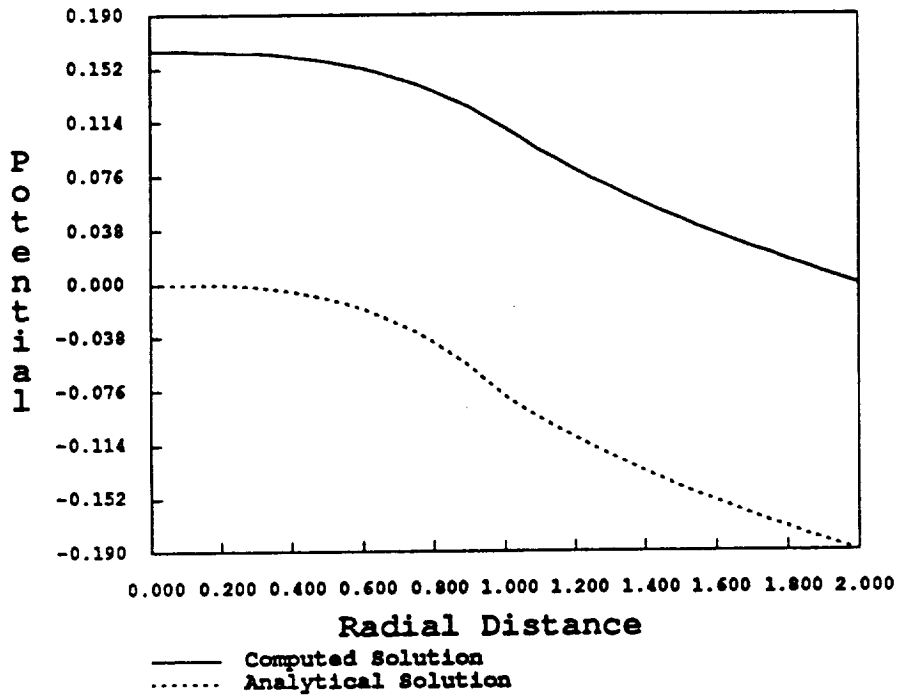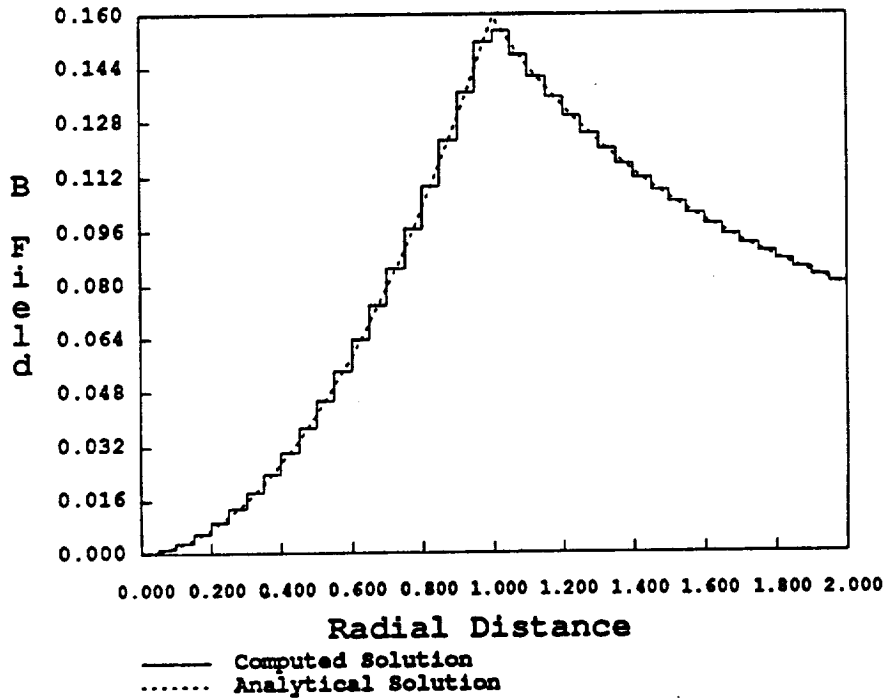B field vs. radial distance, all elements equal conductivities.

Figure 5.
J vs. radial distance, element conductivities equal to element number.
Computed solution plotted as points to highlight accuracy of method in matching exact solution.

38

Figure 6.
A vs. radial distance, element conductivities equal to element number.

Figure 7.
B field vs. radial distance, element conductivities equal to element number.
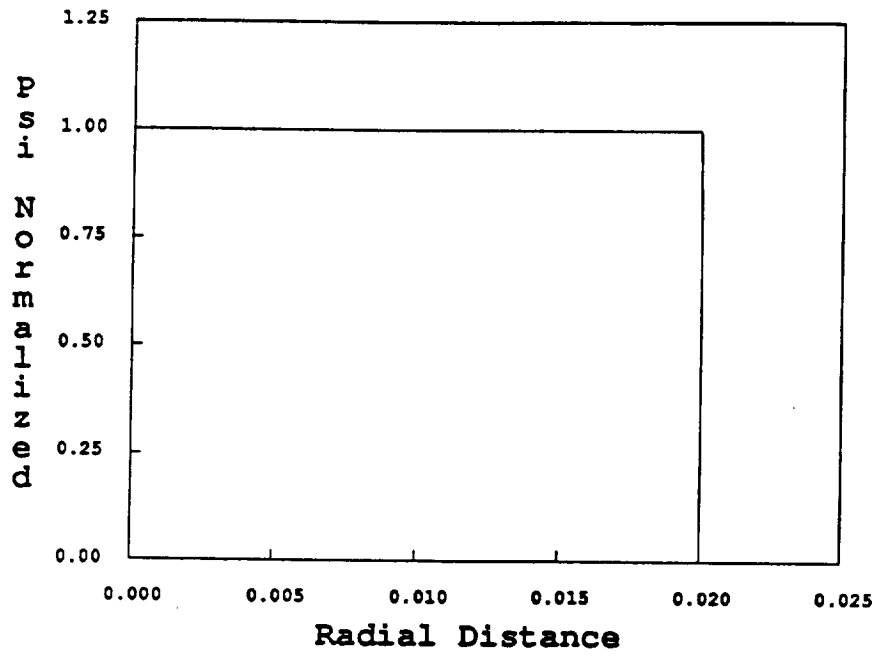
Figure 8.
$|\psi|^2/|\psi_\infty|^2$ vs. radial distance, values for complete mesh plotted.
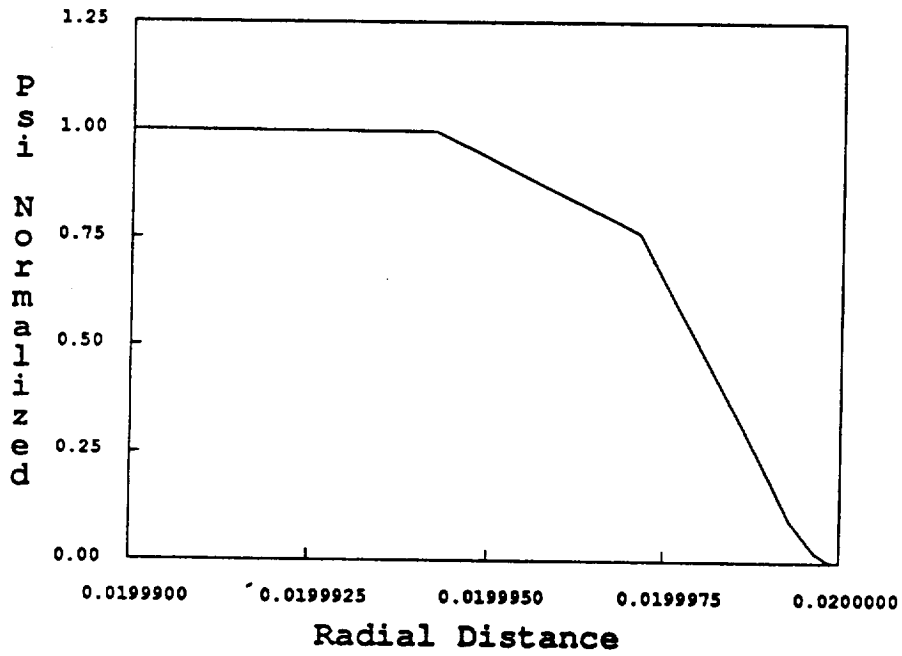
Figure 9.
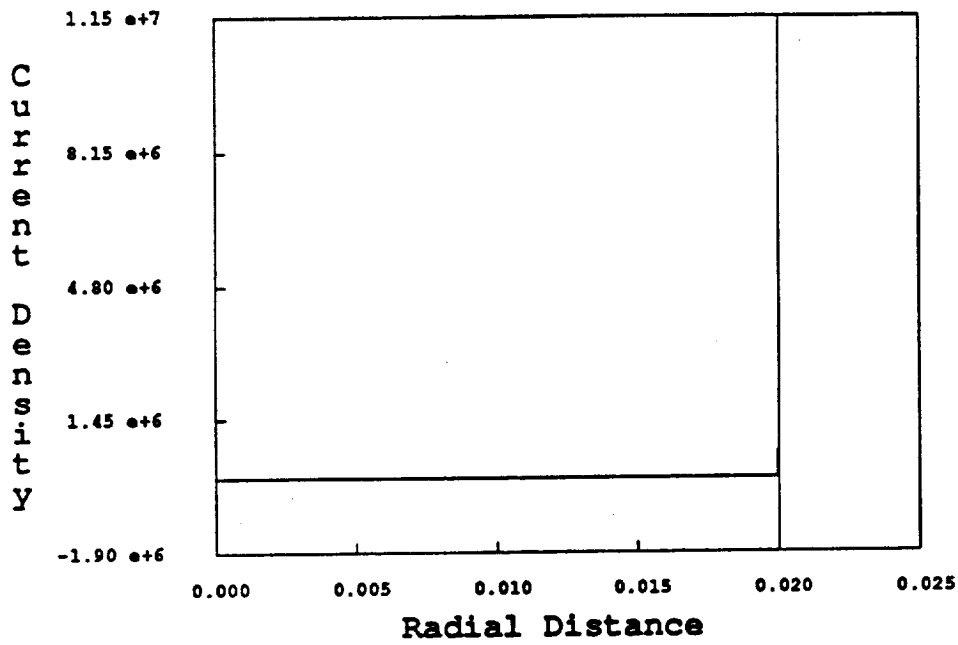$|\psi|^2/|\psi_\infty|^2$ vs. radial distance, values in boundary layer plotted.

Figure 10.
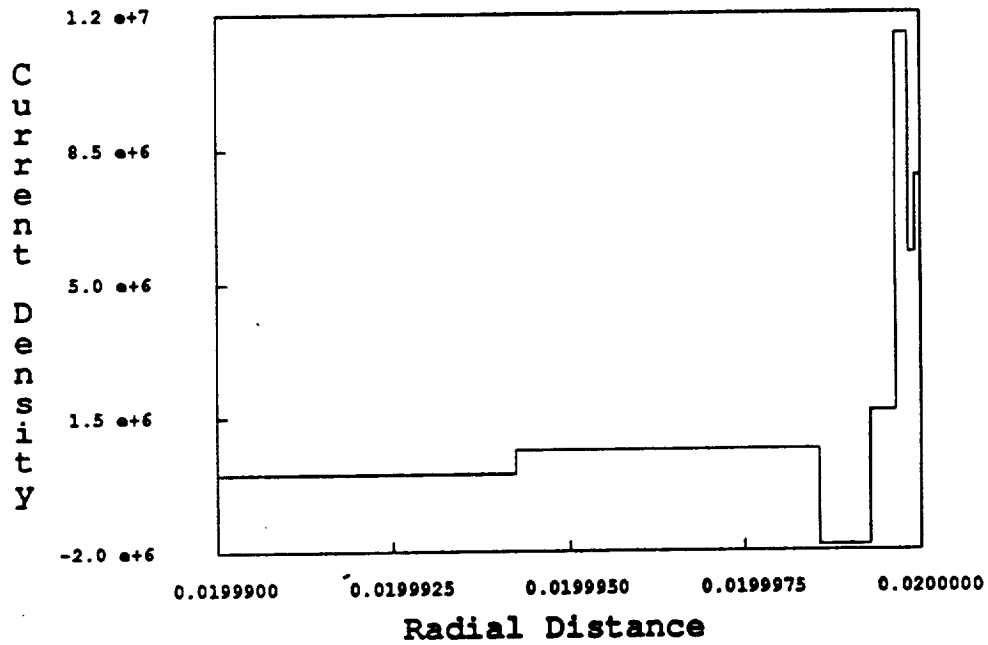J vs. radial distance, values for complete mesh plotted.

Figure 11.
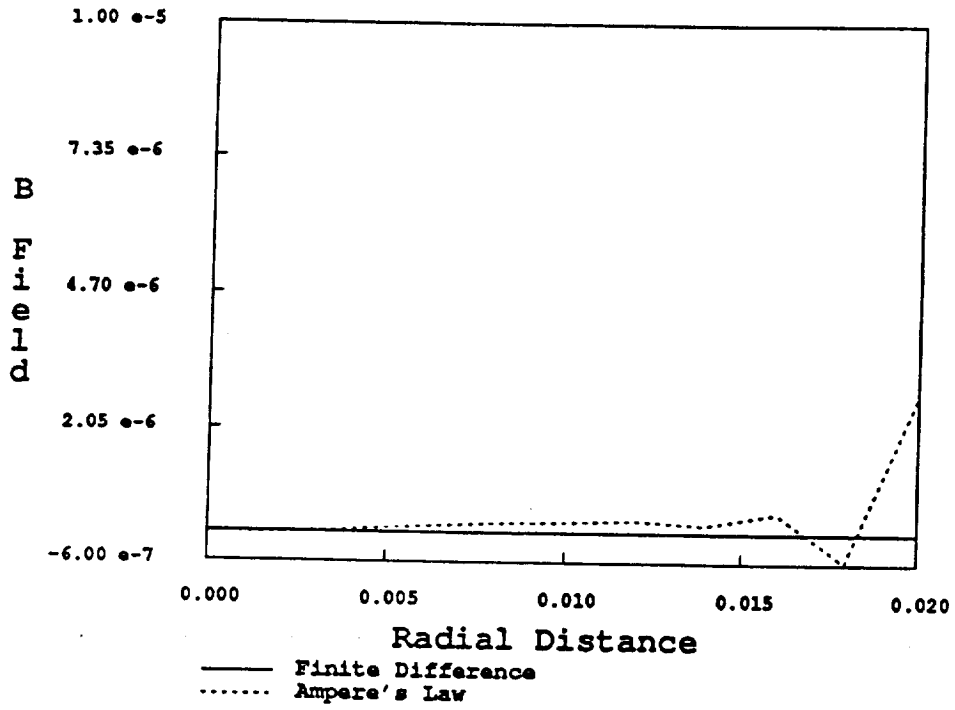J vs. radial distance, values in boundary layer plotted.

41

Figure 12.

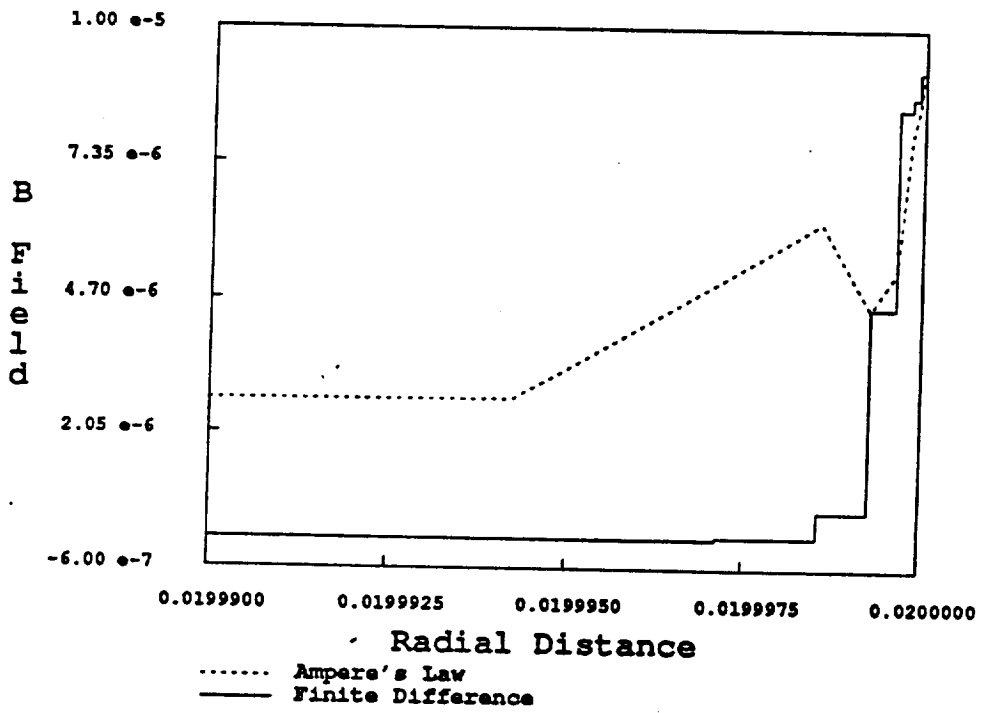B field vs. radial distance, values for complete mesh plotted.

Figure 13.

B field vs. radial distance, values in boundary layer plotted.

REPORT DOCUMENTATION PAGE

Public reporting burden for this collection of information is estimated to average 1 hour per response, including the time for reviewing instructions, searching existing data sources, gathering and maintaining the data needed, and completing and reviewing the collection of information. Send comments regarding this burden estimate or any other aspect of this collection of information, including suggestions for reducing this burden, to Washington Headquarters Services, Directorate for Information Operations and Reports, 1215 Jefferson Davis Highway, Suite 1204, Arlington, VA 22202-4302, and to the Office of Management and Budget, Paperwork Reduction Project (0704-0188), Washington, DC 20503.

1. AGENCY USE ONLY (Leave blank)	2. REPORT DATE December 1991	3. REPORT TYPE AND DATES COVERED Final Contractor Report

4. TITLE AND SUBTITLE

Analysis of Superconducting Electromagnetic Finite Elements Based on a Magnetic Vector Potential Variational Principle

5. FUNDING NUMBERS

WU-505-63-5B
G-NAG-934

6. AUTHOR(S)

James J. Schuler and Carlos A. Felippa

7. PERFORMING ORGANIZATION NAME(S) AND ADDRESS(ES)

University of Colorado
Department of Aerospace Engineering Sciences and
Center for Space Structures and Controls
Boulder, Colorado 80309-0429

8. PERFORMING ORGANIZATION REPORT NUMBER

None

9. SPONSORING/MONITORING AGENCY NAMES(S) AND ADDRESS(ES)

National Aeronautics and Space Administration
Lewis Research Center
Cleveland, Ohio 44135-3191

10. SPONSORING/MONITORING AGENCY REPORT NUMBER

NASA CR-189090
CU-CSSC-91-28

11. SUPPLEMENTARY NOTES

Project Manager, C.C. Chamis, Structures Division, NASA Lewis Research Center, (216) 433-3252.

12a. DISTRIBUTION/AVAILABILITY STATEMENT

Unclassified - Unlimited
Subject Category 39

12b. DISTRIBUTION CODE

13. ABSTRACT (Maximum 200 words)

Electromagnetic finite elements are extended based on a variational principle that uses the electromagnetic four-potential as primary variable. The variational principle is extended to include the ability to predict a non-linear current distribution within a conductor. The extension of this theory is first done on a normal conductor and tested on two different problems. In both problems, the geometry remains the same, but the material properties are different. The geometry is that of a one-dimensional infinite wire. The first problem is merely a linear "control" case used to validate the new theory. The second more interesting problem is made up of linear conductors with varying conductivities. Both problems perform exceedingly well and predict current densities that are accurate to within a few ten-thousandths of a percent of the exact values. The fourth potential is then removed, leaving only the magnetic vector potential, and the variational principle is further extended to predict magnetic potentials, magnetic fields, the number of charge carriers and the current densities within a superconductor. The new element generated by this formulation is then tested on a one-dimensional infinite superconducting wire. The element produces good results for the mean magnetic field, the vector potential and the number of superconducting charge carriers despite a relatively high system condition number. The element did not perform well in predicting the current density. Numerical problems inherent to this formulation are explored and possible remedies to produce better current predicting finite elements are presented.

14. SUBJECT TERMS

Four-potential; Non-linear; Current distribution; Magnetic field; Sample problems

15. NUMBER OF PAGES
44

16. PRICE CODE
A03

17. SECURITY CLASSIFICATION OF REPORT	18. SECURITY CLASSIFICATION OF THIS PAGE	19. SECURITY CLASSIFICATION OF ABSTRACT	20. LIMITATION OF ABSTRACT
Unclassified	Unclassified	Unclassified	